Synoptic Composites of the Extratropical Transition Life Cycle of North Atlantic Tropical Cyclones: Factors Determining Posttransition Evolution

ROBERT E. HART

Department of Meteorology, The Florida State University, Tallahasee, Florida

JENNI L. EVANS

Department of Meteorology, The Pennsylvania State University, University Park, Pennsylvania

CLARK EVANS

Department of Meteorology, The Florida State University, Tallahasee, Florida

(Manuscript received 1 February 2005, in final form 28 June 2005)

ABSTRACT

A 34-member ensemble-mean trajectory through the cyclone phase space (CPS) is calculated using Navy Operational Global Atmospheric Prediction System (NOGAPS) analyses for North Atlantic tropical cyclones (TCs) undergoing extratropical transition (ET). Synoptic composites at four ET milestones are examined: 24 h prior to the beginning of ET ($T_B - 24$), the beginning of ET (T_B), the end of ET (T_E), and 24 h after the end of ET ($T_E + 24$). While the extratropically transitioning TC structure is tightly constrained in its tropical phase, it has a variety of evolutions after $\mathbf{T_E}$. Partitioning the ensemble based upon post-ET intensity change or structure discriminates among statistically significant ET precursor conditions. Compositing the various post-ET intensity regimes provides insight into the important environmental factors governing post-ET development.

A TC that intensifies (weakens) after T_E begins transition ($t = T_B$) with a negatively (positively) tilted trough 1000 km (1500 km) upstream. The negative tilt permits a contraction and intensification of the eddy potential vorticity (PV) flux, while the positive trough tilt prevents contraction and intensification of the forcing. In 6 of the 34 cases, the posttropical cold-core cyclone develops a warm-seclusion structure, rather than remaining cold core. Anticipation of this warm-seclusion evolution is critical since it represents a dramatically increased risk of middle- to high-latitude wind and wave damage. The warm-seclusion evolution is most favored when the scale of the interacting trough closely matches the scale of the transitioned TC, focusing the eddy PV flux in the outflow layer of the transitioning TC. The sensitivity of structural evolution prior to and after T_E illustrated here gives insight into the degradation of global model midlatitude forecast accuracy during a pending ET event.

Eliassen–Palm flux cross sections suggest that ET is primarily driven by the eddy angular momentum flux of the trough, rather than the eddy heat flux associated with the trough. The response of the transitioning TC to the eddy angular momentum forcing is to produce adiabatic ascent and cooling radially inward and beneath the region of the forcing to restore thermal wind balance. In the case of ET, the forcing is maximized lower in the atmosphere, and spread over much greater depth, than in the case of trough-induced TC intensification. Only after T_E is the eddy heat flux forcing as significant as the eddy angular momentum forcing, further supporting a physical foundation for the CPS description of cyclone evolution.

1. Introduction

Over the past 5 yr, the extratropical transition (ET) life cycle has been defined based upon satellite signatures (Klein et al. 2000) and objective measures of dynamic and thermal structure (Evans and Hart 2003). Following ET, tropical cyclones (TCs) can become explosive cold-core cyclones, explosive warm-seclusion cyclones, or simply decay as a cold-core cyclone (Hart 2003; Evans and Hart 2003). Each of these three evolution paths has dramatically different wind and precipitation fields (Bosart et al. 2001) and ocean wave (Bowyer 2000; Bowyer and Fogarty 2003) responses

Corresponding author address: Robert Hart, Dept. of Meteorology, The Florida State University, 404 Love Building, Tallahassee, FL 32306-4520.
E-mail: rhart@met.fsu.edu

associated with it. Furthermore, the envelope of realized intensity is fundamentally related to the structure obtained after ET (Hart 2003), so incorrect forecasts of storm structure have the effect of also degrading the intensity forecasts. Yet, numerical models currently struggle in forecasting the basic nature of TC evolution during and after ET (McTaggart-Cowan et al. 2001; Ma et al. 2003). Indeed, the predictability of the long-wave pattern of the Northern Hemisphere often becomes unusually low when an ET event is upcoming (Jones et al. 2003a,b).

Cyclone evolution following ET may depend on the interaction of at least three components: the remnant TC vortex, the upstream conditions, and the downstream conditions. The role of the remnant TC circulation was found to be only a secondary role in the posttransition intensification for Hurricanes Earl (McTaggart-Cowan et al. 2001) and Irene (Evans and Prater-Mayes 2004; Agusti-Panareda et al. 2004), but it played an essential role in the posttransition intensification of Hurricane Danielle (McTaggart-Cowan et al. 2004). In the cases of both Earl and Irene, the characteristics of the upstream trough (rather than the TC remnant) played a critical role in determining the ET outcome. In such cases, it is possible that cyclone development would have occurred regardless of the presence of the remnant TC. In the case of Earl, McTaggart-Cowan et al. (2003) found that a strong zonal jet immediately downstream of Earl contributed to a "baroclinic mode" of development. Conversely, this downstream zonal jet was upstream of coexisting Hurricane Danielle. This jet orientation led to a northward intrusion of warm, moist air to surround Danielle, leading to a "tropical mode" of development. Similar contrasting cases of development and the role of the TC remnant were found in Hurricanes Felix and Iris (Thorncroft and Jones 2000). In nearly all of these (and other) ET cases, there remained a maximum of equivalent potential temperature even after cold-core structure is obtained. The conditionally unstable cyclone core is a common feature of ET and thus is not alone a useful diagnosis method for determining the post-ET evolution.

As will be discussed in this paper, both Earl and Danielle acquired a warm-seclusion structure after brief periods of cold-core structure and so are atypical examples of ET; the conventional ET case (15/21 here) results in either cold-core decay or intensification. Earl strengthened during ET leading to warm seclusion and then weakened afterward, while Danielle strengthened explosively during and after the warm seclusion. This argues that the warm seclusion was a result of the intensification in the case of Earl, and contributed to the explosive intensification of Danielle. An understanding of the differing precursor conditions that lead to a weakening warm seclusion in one case and an explosively intensifying warm seclusion in the other is critical to an effective ET forecast, as the sensible weather and forecast uncertainty of the explosively intensifying case (Danielle) is much larger than the former situation (Earl). While both types of post-ET warm-seclusion evolution were revealed in Hart (2003), the precursor conditions distinguishing the two remain a mystery.

Sea surface temperature (SST) has also been identified as playing a crucial role during the ET process in some cases (Evans and Prater-Mayes 2004), but the fundamental impact of SST in determining post-ET evolution remains undetermined; this environmental impact will be examined here as well. The role of trough interaction has long been identified as a critical feature driving ET (Brand and Guard 1978; Elsberry 1995; Harr and Elsberry 2000; Hanley et al. 2001; Hart and Evans 2001; Klein et al. 2002; Ritchie and Elsberry 2001, 2003). However, there remain unanswered questions concerning what distinguishes an environment where the trough favorably interacts with the TC versus one where the trough shears and destroys the TC before transition to a tilted, baroclinic system is completed. In their climatology of Atlantic ET events, Hart and Evans (2001) suggest that storms that move directly from an environment supportive of tropical development into an environment supportive of baroclinic development are more likely to survive ET and reintensify than systems that languish in an environment that is not conducive to intensification in either regime. They supported this assertion with climatological fields, but composites and individual case studies are needed to truly validate it.

Fortuitously, 1998–2003 represented a period of increased frequency of North Atlantic ET (42 cases), compared to the 6 yr prior (29 cases). Operational analysis advanced dramatically in quality and in the initialization of the TC structure (Goerss and Jeffries 1994) in the mid–late 1990s due largely to the assimilation of satellite-derived datasets (Caplan et al. 1997; Velden et al. 1998). As a result, we are now in a far improved position to examine in more detail the synoptic, thermal, and dynamic aspects of ET that determine the posttransition evolution. During this 6-yr period, 34 of the 42 cases of Atlantic ET were collected for this study. With this large set of ET cases now available, it is possible to map out the basic progression of ET and post-ET evolutions as a function of the characteristics of the TC and the environmental flow, thus generalizing the revealing case studies of Harr et al. (2000) and McTaggart-Cowan et al. (2001, 2003, 2004).

The goal of the research presented here is to define and distinguish the precursor environments that lead to cases of post-ET weakening, strengthening, and/or cold-core evolution or warm seclusion. The approach is to normalize the TC life cycles of each of these 34 cases using the cyclone phase space (CPS; Hart 2003) characterization of cyclone structure. This framework not only permits objective diagnosis of the posttransition structure (cold core or warm seclusion), but also enables compositing of precursor and subsequent storm environments for similar phase evolutions. This facilitates a detailed examination of the differing nature of underlying interaction between the TC and trough. Further, composites of the precursor environments will provide forecasters with schematics for future cyclone evolution, even in situations of low predictability using the numerical model guidance alone.

The structure of the paper is as follows: datasets and methodology underlying the compositing are discussed in section 2. The composite mean CPS evolution is examined in section 3. In section 4 the subcomposites for the distinct groups apparent within the variability about the CPS mean evolution are examined. A concluding summary is presented in section 5 and suggestions for future research are offered in section 6.

2. Data and methodology

a. Datasets

As demonstrated in Hart (2003), it is preferable to have a dataset resolution of at least 1° for reliable diagnosis of cyclone phase structure—in particular the warm-core subset, which is intrinsically a smaller scale. Thus, while the National Centers for Environmental Prediction–National Center for Atmospheric Research (NCEP–NCAR) reanalyses (Kalnay et al. 1996) provide for an extended length of cases for examination of ET, the 2.5° resolution limits meaningful composites of cyclone phase structure. To remedy the resolution issue, analyses from the operational global models are used here. While the Navy Operational Global Atmospheric Prediction System (NOGAPS) (Hogan and Rosmond 1991) was relatively stable over this period, the NCEP Aviation Model [AVN; now Global Forecast System (GFS; Kanamitsu 1989)] had a significant change in the initialization of the TC vortex in 2000 (Liu et al. 2000). Thus, the storm composites performed here were based upon 1° × 1° resolution NOGAPS operational analyses for the period 1998–2003. During these 6 yr, 34 Atlantic TCs underwent resolvable ET (Table 1) as diagnosed within the cyclone phase space (http://moe.met.fsu.edu/cyclonephase). A few TCs that occurred during this period of time could not be included in the composite either because of data gaps or very poor storm representation.

b. Methodology

1) Overview of cyclone phase space

The cyclone phase space (Hart 2003) is a continuum describing the broad evolution of all synoptic-scale cyclones: tropical, extratropical, subtropical, hybrid, and the transitions among each. This continuum is defined by three parameters: 900–600-hPa thermal wind ($-V_T^L$), 600–300-hPa thermal wind ($-V_T^U$), and 900–600-hPa storm-motion-relative thickness asymmetry (B), all measured within 500-km radius. Positive (negative) values of $-V_T^L$ or $-V_T^U$ indicate a warm- (cold-) core structure in that layer [geostrophic wind and, therefore, isobaric height perturbation (decreasing) increasing with height]. Large positive values of B indicate a highly asymmetric (frontal) cyclone with direct circulation, near-zero values of B indicate symmetry, and large negative values of B indicate occlusion and indirect circulation. By tracing the evolution of a given cyclone within this three-dimensional space, the structural changes of the cyclone can be depicted, including ET (Evans and Hart 2003). The three parameters lead to the formation of a continuum of cyclone structure, which can be grossly described by eight quadrants (Fig. 2). The objective definition of the cyclone evolution provided by the CPS permits the normalization of various cyclone life cycles into a dimensionless time frame, and compositing. The reader is referred to Hart (2003) for a more detailed description of the cyclone phase space.

2) Normalizing the ET time line

The ET life cycle defined in Evans and Hart (2003) is used here, with the beginning of ET (labeled as T_B) as the time when the storm becomes significantly asymmetric ($B > 10$) and end of ET (labeled as T_E) the time when the lower-tropospheric thermal wind indicates a cold core (i.e., $-V_T^L < 0$). These thresholds for beginning and end of transition were confirmed by the objective clustering of transitioning storms in the CPS by Arnott et al. (2004). Since the CPS path is derived from model analyses, T_B and T_E will correspond to the closest analysis time *on or after* these milestones are reached.

To examine the precursor and subsequent synoptic evolution of the cyclones, seven additional times were defined with respect to these two points: $T_B - 72$ h, $T_B - 48$ h, $T_B - 24$ h, T_{MID} [$= ½ (T_B + T_E)$], $T_E + 24$ h, $T_E + 48$ h, and $T_E + 72$ h. This normalizing of the ET time line of each TC enables direct comparison of the evolution of one system to another. While all nine milestones are used to produce a composite mean cyclone phase life cycle, for purposes of brevity only four of the

TABLE 1. North Atlantic transitioning tropical cyclones used in this study. The time taken for each storm to transition ($T_E - T_B$ in hours) is listed in column 2; NHC best-track intensity (MSLP) at T_B in column 3; post-ET intensity change (MSLP from $T_E \rightarrow T_E$ + 24 h) in column 4; the average radius (km) of gale-force (>34 kt) wind from the NHC advisory around T_B in column 5; and post-ET structure, as determined from the CPS, is identified in column 6.

Storm name (year)	Length (h) of transition period	NHC best-track intensity at T_B (hPa)	Best-track MSLP intensity change $T_E \rightarrow T_E$ + 24 h	NHC mean radius of gale force winds at T_B (km)	CPS-determined post-ET structure
Bonnie (1998)	48 (slow)	993	Weakened	245	Cold core
Danielle (1998)	48 (slow)	975	Strengthened	324	Warm seclusion
Earl (1998)	36	994	Weakened	155	Warm seclusion
Ivan (1998)	36	980	Weakened	162	Cold core
Jeanne (1998)	24	1006	Neutral	0	Cold core
Karl (1998)	24	970	Weakened	162	Cold core
Mitch (1998)	36	998	Neutral	220	Warm seclusion
Nicole (1998)	48 (slow)	987	N/A	201	N/A
Cindy (1999)	N/A	984	N/A	231	N/A
Dennis (1999)	N/A	965	N/A	303	N/A
Floyd (1999)	48 (slow)	950	N/A	328	N/A
Gert (1999)	36	964	N/A	378	N/A
Harvey (1999)	N/A	996	N/A	64	N/A
Irene (1999)	12 (fast)	976	Weakened	305	Warm seclusion
Jose (1999)	12 (fast)	987	Weakened	156	Cold core
Alberto (2000)	36	983	Weakened	206	Cold core
Florence (2000)	24	987	N/A	197	N/A
Gordon (2000)	12 (fast)	992	N/A	153	N/A
Isaac (2000)	60 (slow)	979	Weakened	324	Cold core
Michael (2000)	12 (fast)	983	Strengthened	266	Cold core
Nadine (2000)	36	999	Neutral	191	Cold core
Allison (2001)	12 (fast)	1006	Weakened	0	Cold core
Erin (2001)	72 (slow)	979	Strengthened	237	Cold core
Gabrielle (2001)	168 (slow)	983	Neutral	162	Cold core
Humberto (2001)	12 (fast)	970	Weakened	155	Cold core
Karen (2001)	0 (fast)	998	N/A	149	N/A
Michelle (2001)	60 (slow)	947	N/A	245	N/A
Cristobal (2002)	24	1003	N/A	136	N/A
Gustav (2002)	24	971	Weakened	266	Cold core
Isidore (2002)	24	985	N/A	321	N/A
Josephine (2002)	0 (fast)	1009	Strengthened	35	Cold core
Fabian (2003)	96 (slow)	962	Strengthened	301	Warm seclusion
Isabel (2003)	12 (fast)	969	N/A	370	N/A
Kate (2003)	12 (fast)	987	Strengthened	254	Warm seclusion

nine milestones are examined here and illustrated with the synoptic composites: T_B − 24 h, T_B, T_E, and T_E + 24 h.

3) Compositing

For each cyclone, a storm-relative 1° × 1° resolution grid, spanning 91° of longitude and 91° of latitude, was centered over the cyclone center; only a subset of this grid will be shown here to focus on the region of interest. In regions where this grid reached over the North Pole or below the equator, that region of the grid was set to missing values to avoid contaminating the eventual composite. The NOGAPS-based storm-relative grid was then produced for each of the four ET milestones defined above. After this process was repeated for each of the 34 cyclones, the composite mean storm-relative grid was produced. No attempt was made to rotate the storm-relative grid based upon storm motion. Thus, direction of storm-motion sensitivity in ET evolution will not be resolved in this analysis.

4) Eliassen–Palm flux calculations

The Eliassen–Palm (EP) flux is calculated for the mean environment for each of the five partitions for which synoptic composites were developed: full composite, cold core, warm seclusion, strengthening, and weakening subcomposites. Data for each member of each composite are obtained from NOGAPS analyses over a 51° latitude by 51° longitude grid centered over the surface center of each storm [defined by minimum in mean sea level pressure (MSLP)] and converted to a cylindrical grid extending out to a radius of 1500 km from the center of each storm ($\Delta r = 50$ km, $\Delta\lambda = \pi/6$ radians). Mean synoptic environments for each composite are developed and calculations of the EP flux for these environments are made following the storm-relative framework outlined by Molinari et al. (1995). The EP flux includes components of the eddy heat and momentum fluxes and its divergence is a direct measure of the eddy potential vorticity (PV) flux. Eliassen–Palm flux vectors pointing outward (inward) indicate inward (outward) eddy angular momentum flux. Upward (downward) pointing vectors indicate inward (outward) eddy heat flux. Thus, the EP flux vector, and the resulting eddy PV flux its divergence implies, are useful tools to diagnose the magnitude and significance of the asymmetric, external forcing upon a assumed symmetric TC vortex as it undergoes ET.

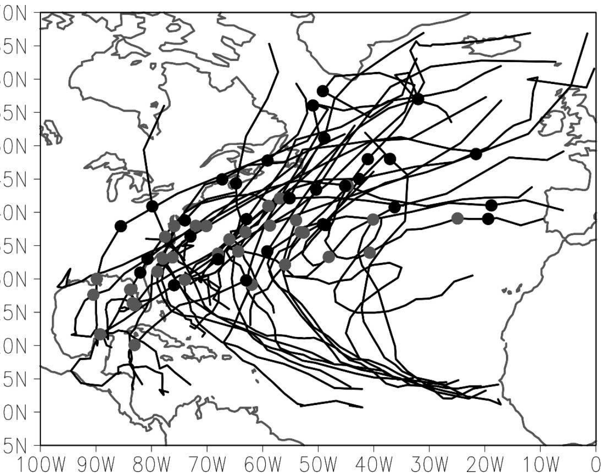

FIG. 1. Tracks of the 34 composited tropical cyclones spanning 1998–2003 described in Table 1. Gray circle indicates the start of extratropical transition (T_B), and black circle indicates the end of extratropical transition (T_E).

5) IMPACT OF NOGAPS BOGUS

The NOGAPS TC initialization includes the insertion of a synthetic vortex. This vortex is blended with the environmental pattern in such a way that it is not simply an idealized, perfectly symmetric TC inserted within a real environment (Goerss and Jeffries 1994). The consequence of the NOGAPS TC initialization process is that the cyclone itself is in balance not only with itself, but is reasonably in balance with the environmental flow. Thus, a NOGAPS TC undergoing ET is not simply a perfectly symmetric warm-core cyclone within a highly asymmetric, baroclinic environment. Instead, it is an asymmetric, warm-core vortex. The extent to which this is a successful merger is not well documented, however.

3. Composite mean evolution and ET variability

The transition locations of the 34 cyclones composited (Fig. 1) illustrate the great range of latitude and longitude that ET encompasses, highlighting the need for storm-relative coordinates in the compositing. The diversity of CPS evolutions in ET (Fig. 2) demands detailed scrutiny of the environments in which ET occurs. These are examined next in the context of a composite CPS and variation around the mean CPS path, followed by compositing of the storm environments at the key stages highlighted above in the ET process.

a. *Composite mean cyclone phase evolution*

The 34-storm composite mean cyclone phase evolution is depicted in Fig. 3; the nine key milestones are highlighted in Table 2. The mean evolution of cyclone structure from symmetric warm core, to hybrid, to asymmetric cold core, to eventual occlusion is well illustrated. The average transitioning TC peaks in warm-core intensity around 24 h prior to the start of ET (T_B – 24 h with $-V_T^L \approx 100$). This result is consistent with Hart and Evans (2001) and illustrates why a significant percentage of Atlantic TCs are capable of undergoing ET in the first place. Complete dissipation of a TC from peak intensity generally takes several days, yet a TC only has to survive for 24 h after weakening from peak intensity to reach a baroclinic environment supporting the commencement of ET. In basins where ET is less common (the south Indian Ocean, for example), the peak warm core intensity of the cyclone would be expected to occur several days prior to T_B [e.g., the "captured" cyclones of Foley and Hanstrum (1994)], making survival to ET less common. Further, with a more zonal long-wave pattern in the Southern Hemisphere, the scale matching between the trough and TC that is necessary for constructive interaction (Molinari et al. 1995; Hanley et al. 2001; section 4) is less likely to be achieved than in the more meridionally amplified Northern Hemisphere.

Within 24 h of transition completing (T_E + 24 h), the North Atlantic cyclone has achieved its largest value of B and also has significantly decreased in pressure (Fig. 3). The former suggests that upon completion of ET the mean cyclone has reached the strongest storm-motion-relative temperature gradient it will attain. One to two days after this, the cyclone has continued to intensify and expand considerably in size, with B decreasing as

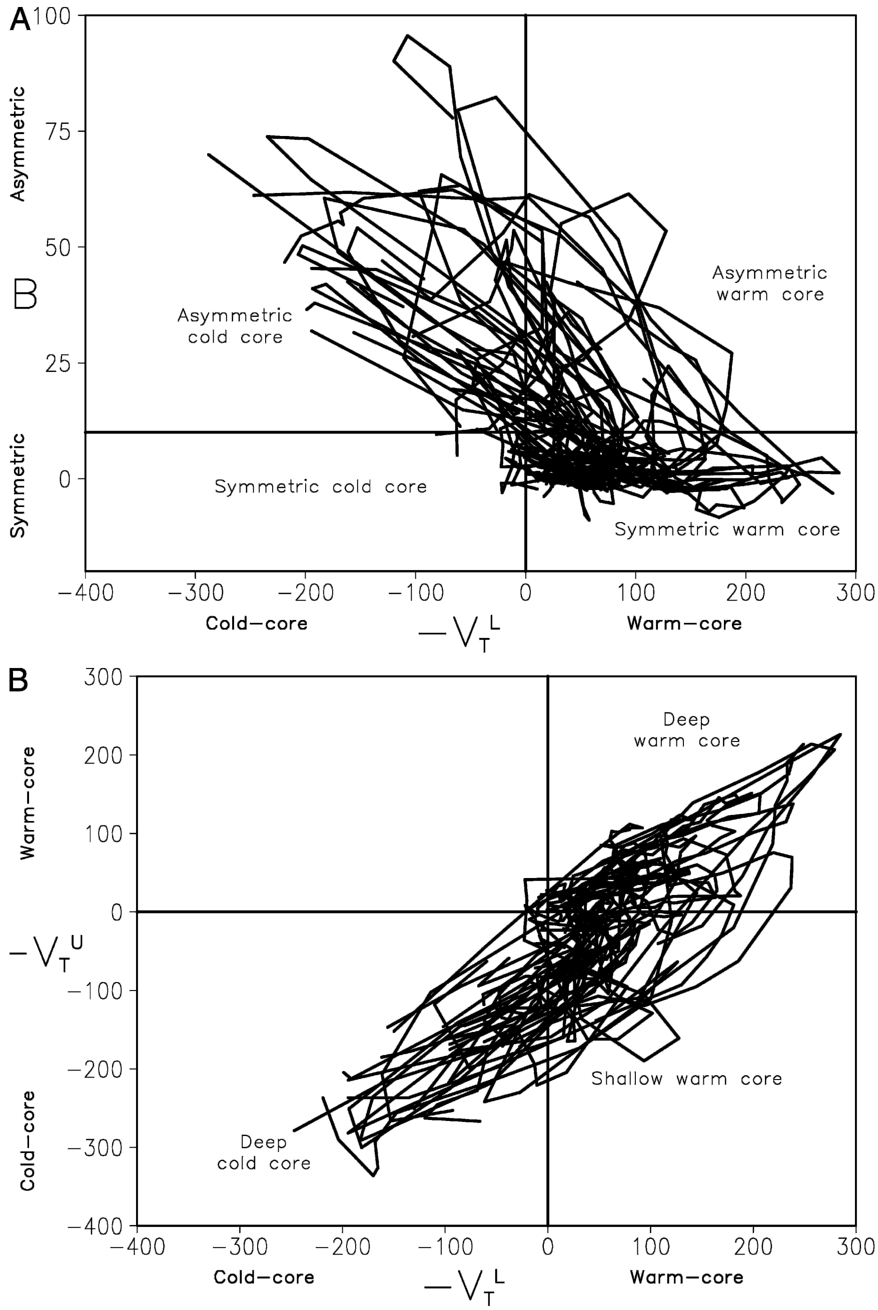

FIG. 2. Spaghetti plot of cyclone phase evolution of the 34 composited storms: (a) B vs $-V_T^L$ and (b) $-V_T^L$ vs $-V_T$. The CPS is defined in Hart (2003), where $-V_T^L$ is the scaled 900–600-hPa thermal wind and B is the 900–600-hPa storm-motion-relative thickness asymmetry.

the baroclinic instability is removed. Soon after $T_E + 72$ h, the occlusion process has begun (not shown).

b. Composite mean synoptic evolution during ET

Storm relative composites of the evolution of the mean transitioning cyclone are shown in Figs. 4–8. The mean evolution from $T_B - 24$ h to $T_E + 24$ h involves the approach of a positively tilted trough that interacts with the TC, ultimately merging with it by the end of transition.

Prior to the start of transition ($T_B - 24$ h), the TC has commenced recurvature, but remains distinct from the midlatitude environment (Figs. 4a, 6a). The storm's tropical connection is also evident in the equivalent po-

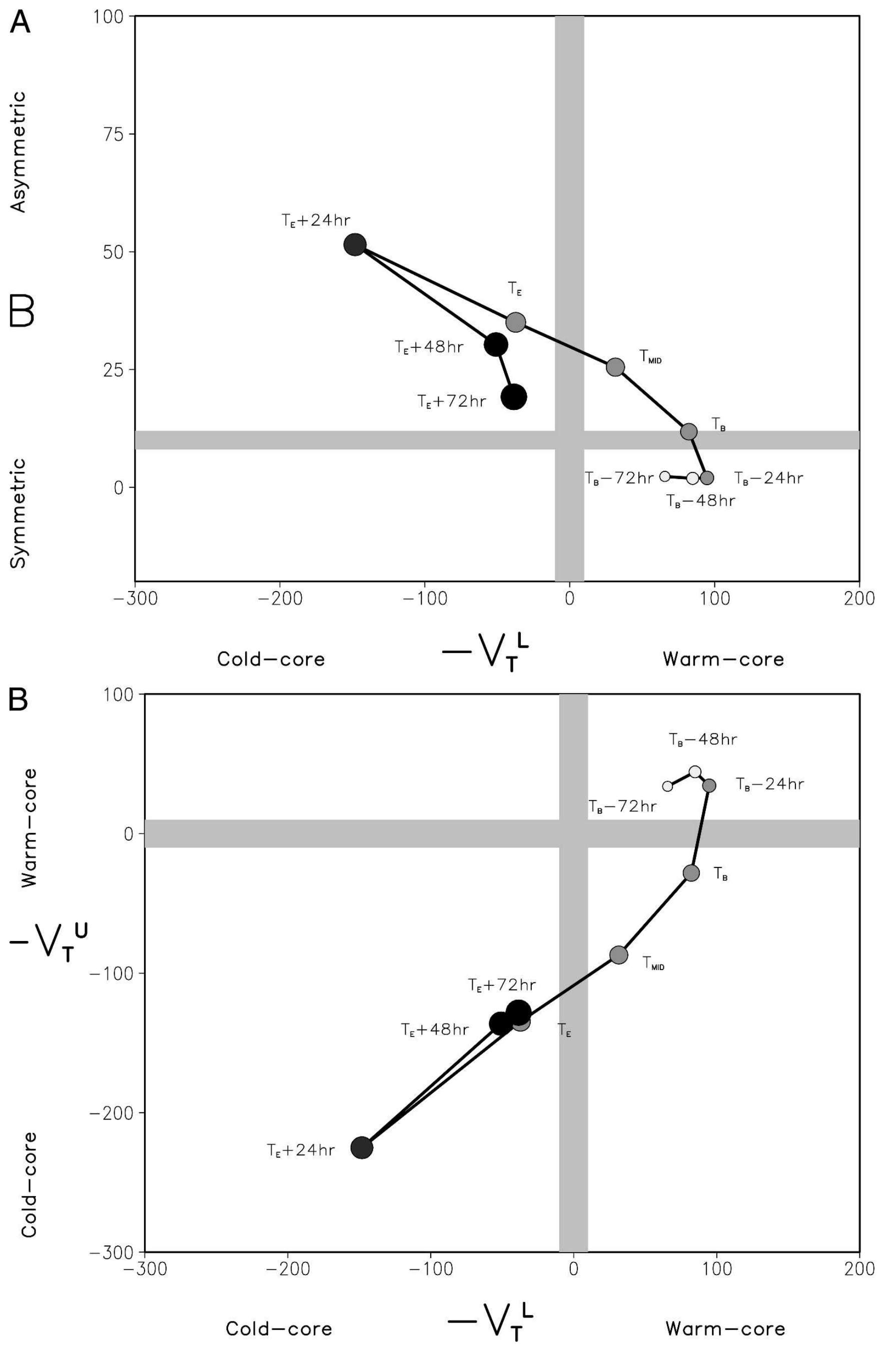

FIG. 3. The 1998–2003 34-cyclone composite mean cyclone trajectory using NOGAPS 1° analysis: (a) B vs $-V_T^L$ and (b) $-V_T^L$ vs $-V_T^U$. Here T_B and T_E represent the start and end of ET, respectively, as defined in Evans and Hart (2003), and T_{MID} represents the midpoint of ET. The size of the circular marker indicates the average radius of 925-hPa gale-force winds, from 225 km at $T_B - 72$ h to 570 km at $T_E + 72$ h. The gray shading of the marker indicates minimum mean sea level pressure, from 1001 hPa at $T_B - 72$ h to 982 hPa at $T_E + 72$ h. The numbers of available cases for each of the nine times above are 33, 34, 34, 34, 31, 31, 26, 17, and 11. For reasons of brevity, only four of the milestones will be examined here: $T_B - 24$ h, T_B, T_E, and $T_E + 24$ h. Gray bars are the general division among the four cyclone phase quadrants in each figure.

TABLE 2. Mean and standard deviation (in parentheses) for key storm characteristics for the nine milestones identified for ET evolution.

	Minimum sea level pressure (hPa)	Radius of gale-force 925-hPa wind (km)	B	$-V_T^L$	$-V_T^U$
$T_B - 72$ h	1000.8	226.0	2.3	65.7	33.9
	(10.6)	(183.4)	(5.6)	(67.0)	(62.2)
$T_B - 48$ h	997.8	267.9	1.9	84.9	44.3
	(11.0)	(192.9)	(5.0)	(70.0)	(73.1)
$T_B - 24$ h	996.6	298.2	2.0	94.8	34.4
	(10.4)	(192.5)	(3.6)	(66.8)	(70.6)
T_B	995.2	368.2	11.8	82.3	−28.2
	(7.8)	(151.5)	(5.1)	(62.7)	(64.7)
T_{MID}	994.2	405.7	25.5	31.6	−87.0
	(9.6)	(192.4)	(13.2)	(66.3)	(64.1)
T_E	995.0	440.4	35.0	−37.2	−134.6
	(10.5)	(239.8)	(21.0)	(55.0)	(73.5)
$T_E + 24$ h	990.5	494.8	51.5	−148.1	−225.1
	(12.5)	(260.2)	(28.7)	(146.4)	(115.5)
$T_E + 48$ h	985.6	524.8	30.3	−50.8	−136.2
	(15.2)	(324.4)	(29.5)	(119.8)	(130.1)
$T_E + 72$ h	982.3	571.4	19.2	−38.5	−128.3
	(15.9)	(352.8)	(21.5)	(95.7)	(88.3)

tential temperature field (Fig. 5a). While this connection has weakened by the start of transition (Fig. 5b), the local minimum of static stability associated with the TC (Figs. 5a, 7a) serves to enhance the Eady baroclinic growth rate, σ (Eady 1949; $\sigma = fU_Z N^{-1}$), of the environment between the trough and TC. Because of the decreased static stability, the trough is effectively made a more dynamically deep baroclinic system through the introduction of the TC and its environment (Harr et al. 2000). Although not shown, the lifting of the tropopause ahead of the trough by the TC's anticyclone increases the baroclinicity of the upper troposphere, leading to enhancement of the jet streak that is typically found with the trough.

By the end of transition (Fig. 5c) the moist, unstable core of the remnant TC has weakened considerably; however, a local maximum of 850-hPa equivalent potential temperature at the end of transition (Fig. 5c) is consistent with Thorncroft and Jones (2000). The remnant maximum of moisture in the presence of a pressure minimum without a larger maximum of temperature illustrates why equivalent potential temperature alone cannot be used as an indicator of warm- versus cold-core structure in cyclones.

A potential vorticity perspective on the ET life cycle (Figs. 6 and 7) illustrates the approach of the trough while the low-level PV maximum of the TC is maintained. Since the 300-hPa static stability of the atmosphere is approximately 20% less immediately surrounding the cyclone than between the cyclone and the approaching trough (dotted contours in Figs. 7a,b), the TC introduced an environment at upper levels that enhanced the Eady baroclinic growth rate of the wave (Fig. 7). By the end of transition (Fig. 7c), the TC has interacted with the trough (the nature of which will be discussed next), with the 0.75-PVU contour extending below 500 hPa by the completion of ET (Fig. 7c). At the same time, the surface cyclone has expanded in size (Figs. 6c, 7c). By 24 h after transition, there is no distinction between the former TC remnant and the trough that interacted with it (Fig. 7d).

To illustrate more clearly the trough's forcing upon the TC, the Eliassen–Palm flux analysis in cylindrical–isentropic coordinates of Molinari et al. (1995) and Harr et al. (2000) was performed (Figs. 8a–d) using the mean atmospheric state of the 34-cyclone composite for each of the four key ET milestones highlighted here: T_B – 24 h, T_B, T_E, and T_E + 24 h. From these analyses, we can determine the relative contribution of the trough in the eddy angular momentum and eddy heat flux forcing (and, implicitly, the eddy potential vorticity flux) within the transitioning TC. Comparisons to the Elena (1985) trough interaction analyses described in Molinari et al. (1995) and the case studies of Harr et al. (2000) can also be drawn.

One day prior to the start of transition (Fig. 8a), there is evidence of weak inward eddy angular momentum flux beyond 1000-km radius in the middle troposphere, resulting from the approaching trough (Fig. 6a). Through ET (Figs. 8b,c), the magnitude of eddy angular momentum flux (horizontal vector) increases markedly, leading to an EP flux divergence and inward flux of eddy PV (shading) throughout the entire storm above 315 K and between 350- and 1500-km radius. Even through T_E, the vast majority of the EP flux divergence is a result of the eddy angular momentum flux rather than the eddy heat flux given the predominant horizontal orientation of the vectors and minimal change in vector magnitude beyond 750-km radius. Although requiring more detailed evaluation with numerical modeling, this result suggests that the conversion of the TC from warm core to cold core is predominantly a consequence of the eddy momentum forcing rather than the eddy heat flux. While this may appear paradoxical at first, it is a natural consequence of the time line of evolution of trough interaction and the trough/TC separation distance throughout. As shown in Fig. 6, the TC completes ET (Fig. 6c) well before merger (Fig. 6d). Given that the majority of the cold air associated with the trough still has not reached the greater part of the storm circulation in Figs. 5b,c, it is

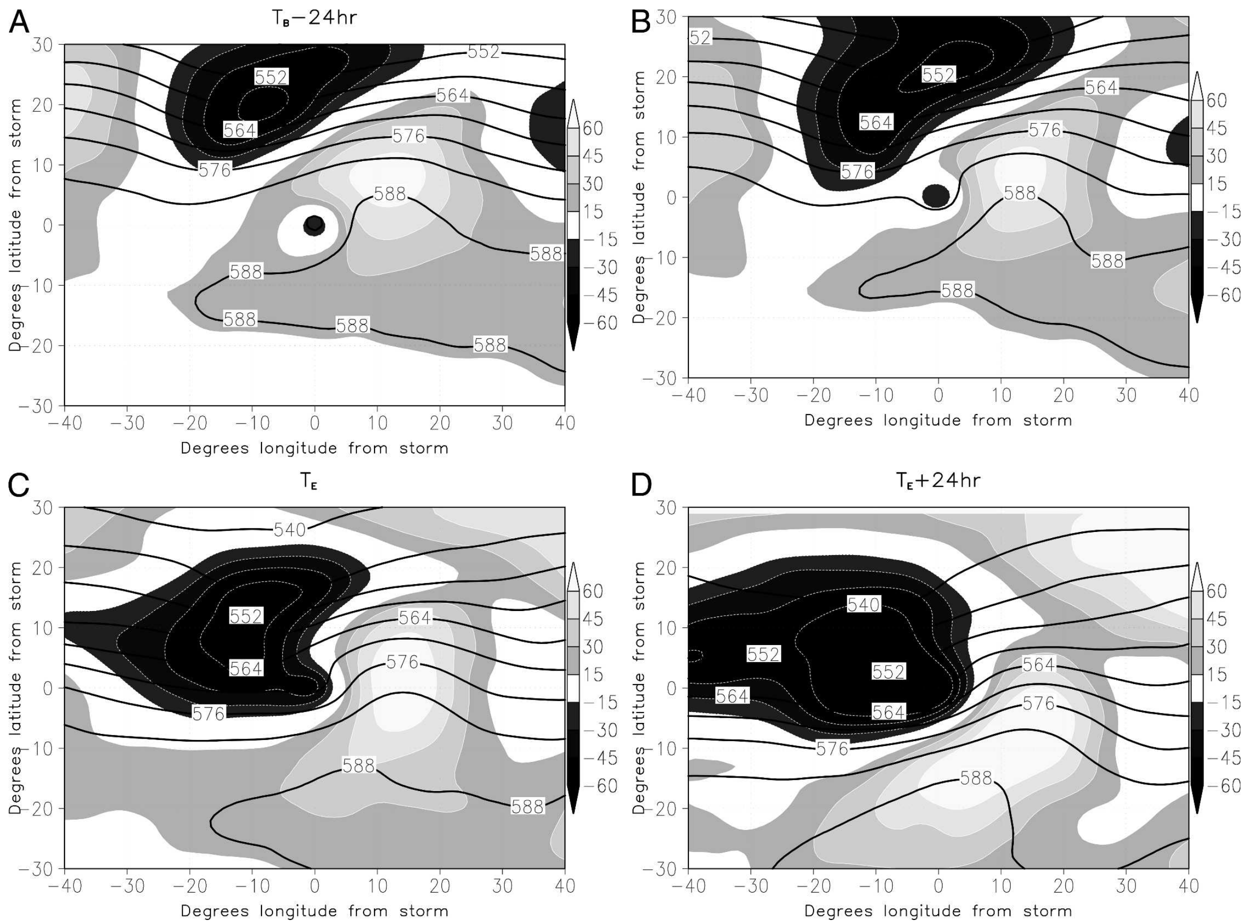

FIG. 4. Composite mean 500-hPa height (contour, dm) and anomaly from monthly mean (shaded, m) for (a) $T_B - 24$ h, (b) T_B, (c) T_E, and (d) $T_E + 24$ h. The transitioning storm is located at (0, 0) in each panel.

not surprising that the magnitude of the eddy heat fluxes at time T_E are small (Fig. 8c).

Molinari et al. (1995) found that in the trough-induced intensification of Hurricane Elena (1985), the eddy angular momentum forcing was maximized around 345 K. The consequence of this forcing was to weaken the anticyclonic circulation aloft, decreasing the vertical wind shear and destroying the TC's thermal wind balance. In an attempt to regain thermal wind balance, the TC response is to produce a couplet of circulation centered on the eddy angular momentum forcing: direct below and indirect above, with enhanced inflow above and below and enhanced outflow in the region of the momentum flux forcing. This leads to adiabatic motion in the troposphere that restores thermal wind balance. Molinari et al. (1995) further argue that the adiabatic motion acts as a trigger to enhance the TC secondary circulation, and increase convection and diabatic warming aloft, intensifying the storm.

In the case of the ET composite in Figs. 8a–d, the eddy angular momentum forcing is centered considerably lower in the atmosphere (330–336 K—approximately 500 hPa), is also much broader in depth, and is located at larger radii. With a deeper and lower layer of eddy momentum flux forcing, the response of the TC wind field will be to cyclonically accelerate the entire outer wind profile under the influence of the eddy angular momentum flux from the trough. In the lower troposphere the adiabatic response would be cooling at inner radii, while in the upper troposphere the adiabatic response would be cooling at larger radii. Given the convergent TC circulation in the lower troposphere, this adiabatic cooling would presumably drive frontogenesis, consistent with Harr and Elsberry (2000) and Harr et al. (2000). It is this adiabatic cooling that leads to the increase in the value of B in the cyclone phase space depiction. This is not to say that preexisting frontal zones cannot also accelerate or initiate the ET process; however, the composite mean of 34 cyclones argues that the adiabatic cooling response from the eddy

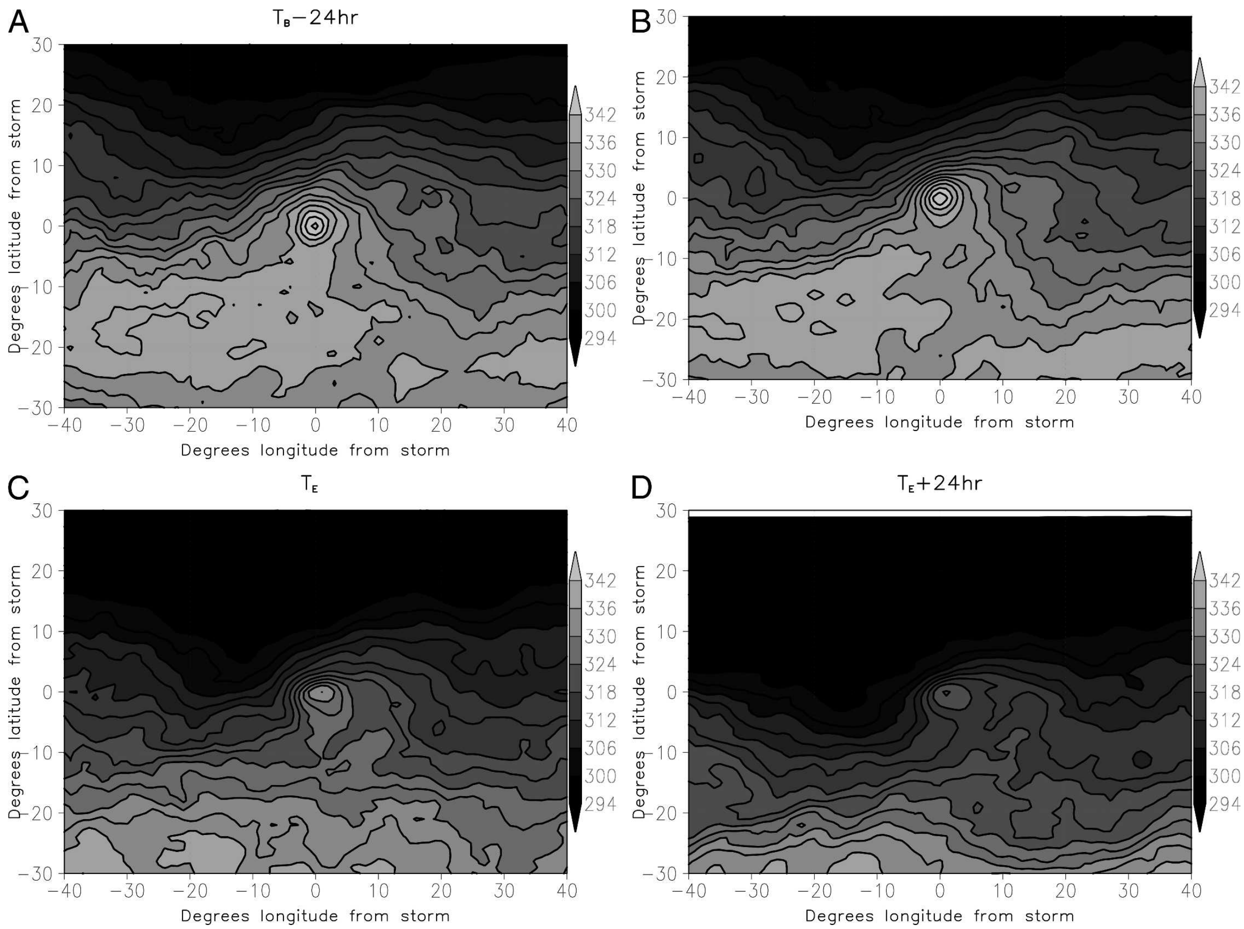

FIG. 5. The 850-hPa equivalent potential temperature for (a) T_B – 24 h, (b) T_B, (c) T_E, and (d) T_E + 24 h.

angular momentum flux in the outer circulation far precedes it, when an upper-atmospheric trough is present.

One day after transition (Fig. 8d), we now see a classic eddy-forcing pattern for an extratropical cyclone with strong inward eddy PV flux between 750 and 1000 km, and outward eddy PV flux above 340 K. The magnitudes of eddy heat and momentum fluxes have increased dramatically, with an intense direct circulation typical of an extratropical cyclone. The EP flux vectors above 350 K are directed almost exclusively downward, suggesting the eddy heat flux is overwhelming the momentum flux at upper levels. This intense outward eddy heat flux is the result of the initially upright vortex tilting westward with height as it becomes baroclinic, such that the cyclone center is no longer aligned at all levels with the cylindrical coordinate used in the EP flux calculations. With the cylindrical coordinate system no longer collocated with the cyclone center aloft, the eddy heat flux is exaggerated with respect to the actual cyclone center.

A comparison of Fig. 8c to Fig. 8d is additional evidence that the cyclone phase space correctly diagnoses the time line of evolution from a tropical to baroclinic structure, since eddy heat fluxes (and, therefore, the westward tilt of the cyclone) are minimal until after T_E is reached (transition to cold core completed).

4. Factors distinguishing transition extremes

Although the mean cyclone evolution just examined is revealing, it fails to elucidate the variability that exists from case to case in the ET life cycle. While variability in the hours leading up to the start of ET is relatively small (Figs. 9a,b; Table 2; $T_B - 24$ h to T_B), variability once ET has commenced increases dramatically (Figs. 9a,b; Table 2; T_E to $T_E + 24$ h). The CPS variability can be further characterized by examining the various cyclone phase space evolutions for representative members of the 34-cyclone composite (Fig. 10). Hurricane Floyd (1999; Fig. 10a) represents a case where the post-ET evolution is one of cold-core decay, while Hurricane Erin (2001; Fig. 10b) represents a case where the

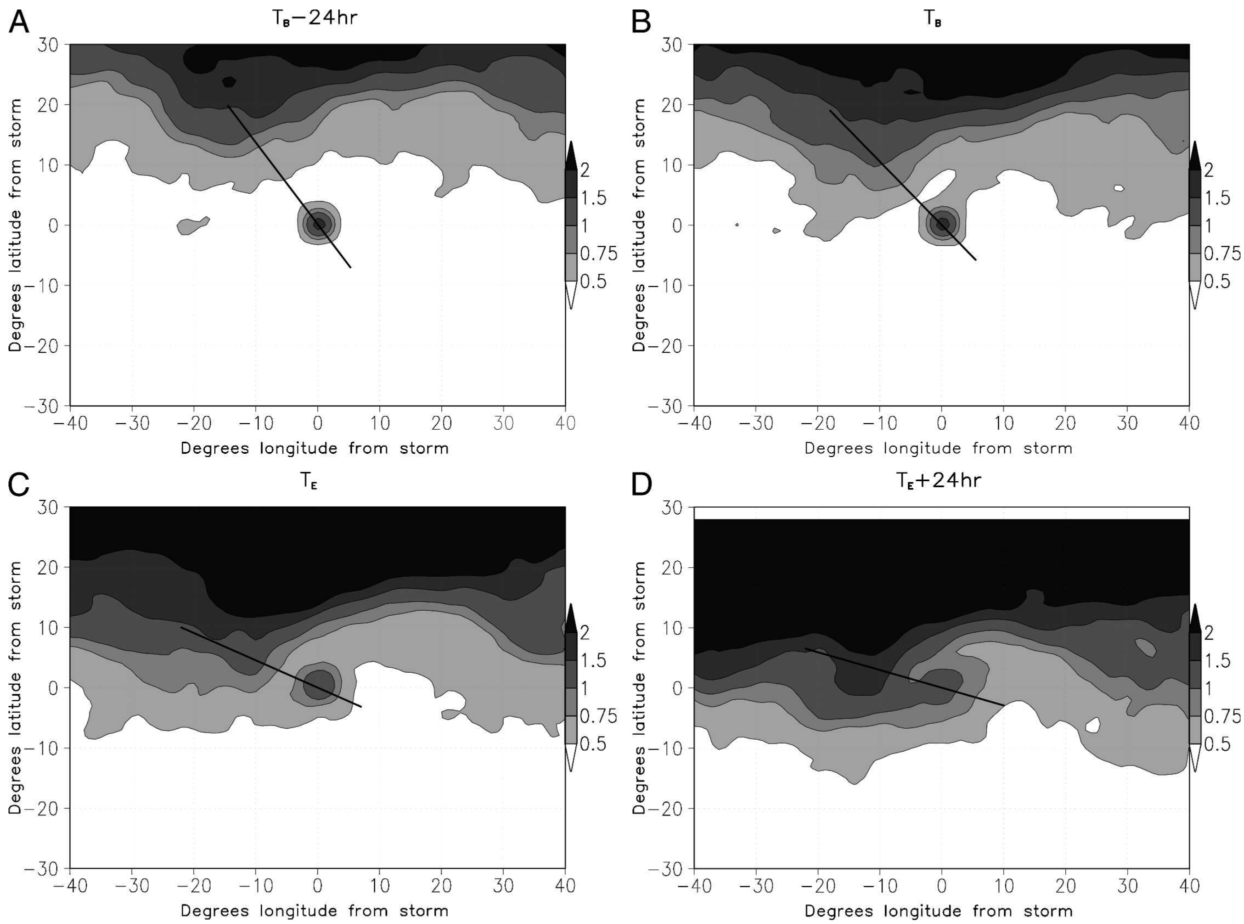

FIG. 6. The 320-K isentropic potential vorticity (shaded, PVU) for (a) $T_B - 24$ h, (b) T_B, (c) T_E, and (d) $T_E + 24$ h. Solid line in each panel is the axis of the cross sections in Fig. 7.

post-ET evolution is one of cold-core intensification. While most TCs take less than 36 h to complete the transition process (Evans and Hart 2003), occasionally the transition process can take several days. Hurricane Gabrielle (2001; Fig. 10c) is one example of a slow-transitioning TC. Occasionally, a transitioned TC can undergo warm seclusion and rapid post-ET reintensification. In these cases, a pocket of warm air is trapped (secluded) in the center of the circulation (Shapiro and Keyser 1990). This structural change has very significant implications that will be discussed. An example of such an evolution is Irene (1999; Fig. 10d). Although not shown, a warm seclusion can occasionally lead to weakening, as happened with Earl (1998). Less frequently, a TC can begin ET, but not complete the process of transition, ultimately regaining tropical structure. In the case of Hurricane Dennis (1999; Fig. 10e), the TC moved back equatorward into a region of decreasing shear and passed over the Gulf Stream, reversing the structural changes toward baroclinic development. Finally, a TC can begin the process of ET but be absorbed by a preexisting extratropical cyclone or be sheared apart before transition completes [e.g., Hurricane Cindy (1999); Fig. 10f].

The nature of posttransition evolution is fundamentally key to the ultimate impact the cyclone will have on both marine and overland interests. The radius of gale-force winds (symbolized by the size of the circles along the CPS path) varies greatly in each of the cases shown in Fig. 10, and even in the mean of each subcomposite type (Table 3). Further, the intrinsic predictability (whether physical or numerical) of the transitioning cyclone varies depending upon the evolution taken. Jones et al. (2003b) have shown that the global long-wave pattern predictability becomes dramatically decreased when a TC moves into the middle latitudes. Since numerical models often have difficulty handling the details of transition and posttransition evolution effectively, it would be helpful to determine and understand the patterns favorable for the various types of cyclone

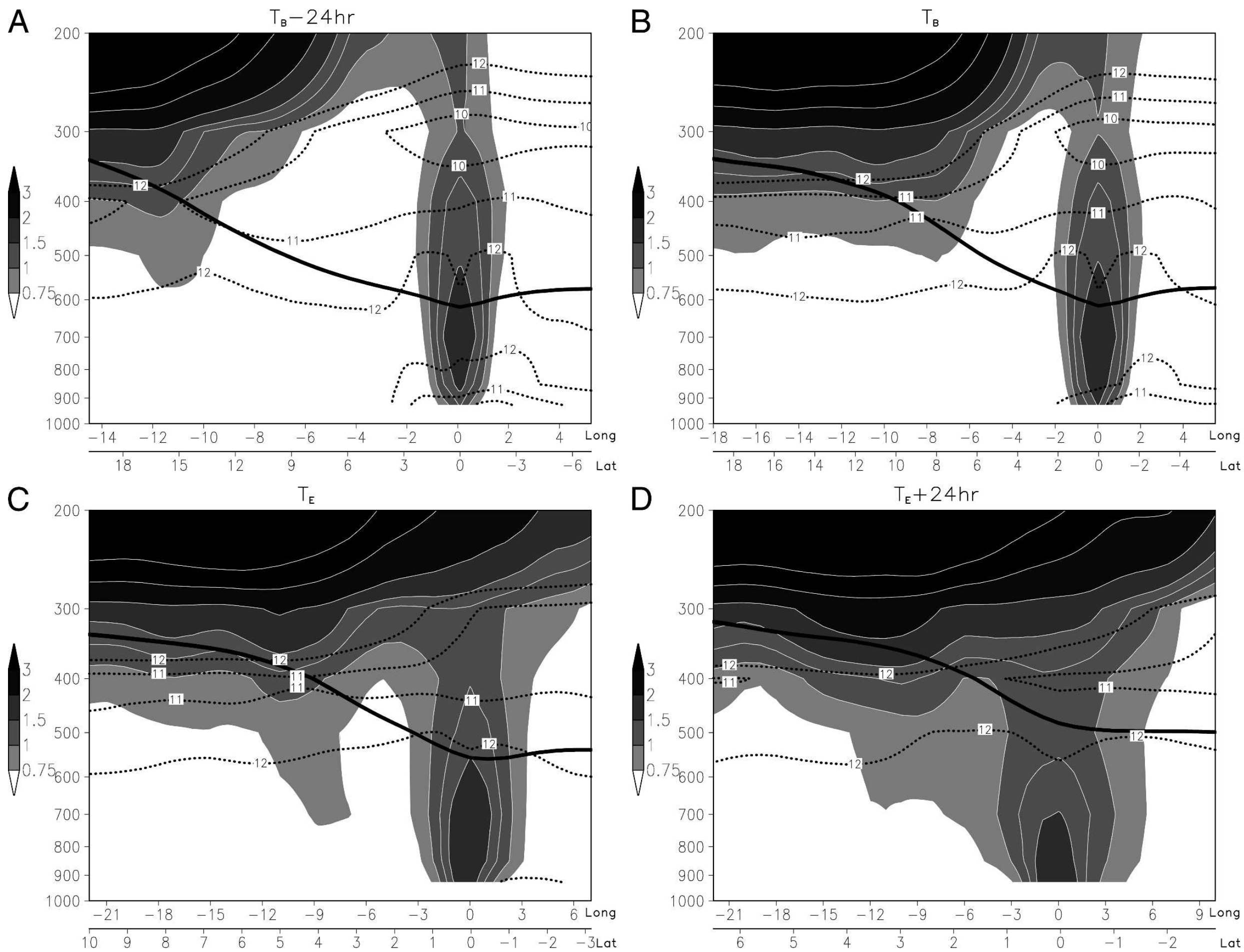

FIG. 7. Cross sections (locations shown in Fig. 6) of potential vorticity (shaded, PVU), 320-K isentropic surface (solid contour), and Brunt–Väisälä frequency (dotted contour, $10^{-2}\ s^{-1}$) for (a) $T_B - 24$ h, (b) T_B, (c) T_E, and (d) $T_E + 24$ h.

evolutions shown in Fig. 10. To isolate these patterns responsible and to understand the environments determining ET evolution and post-ET intensity and structural change more fully, we next examine synoptic subcomposites for six sets of contrasting evolutions.

a. Rapid- ($T_B \rightarrow T_E \leq 12$ h) versus slow- ($T_B \rightarrow T_E \geq 48$ h) transitioning TCs

While the average length of time taken for ET to complete is approximately 30 h (Evans and Hart 2003), there is considerable variability in the time taken to transition (Table 1). To understand the environments that distinguish rapid-transitioning TCs (9 cases from Table 1) from slow-transitioning TCs (10 cases from Table 1), composites of each group at T_B are examined (Fig. 11).

Rapid-transitioning TCs are associated with a higher-amplitude trough than slow-transitioning TCs (Fig. 11). Thus, slow-transitioning TCs are advected zonally across the Atlantic rather than meridionally. Further, slow-transitioning TCs occur over SST about 3°–4°C warmer than rapid-transitioning TCs, and are 10 hPa deeper than fast-transitioning TCs at T_B (Table 3). It is noteworthy that the mean SST for slow-transitioning TCs is 26.5°C, suggesting that, in the mean, the oceanic environment may still remain conducive to tropical development while ET is occurring. The highly amplified trough, typical of rapid-transitioning TCs, steers the TC down the SST gradient; the weaker trough associated with slow-transitioning TCs steers the TC roughly parallel to an SST isotherm. Should the unstable thermodynamic core coexist with SST of 26°–27°C within a baroclinic environment, both modes of development are possible and would compete for structural change, delaying ET completion (Hart and Evans 2001).

In the mean, a rapid- (slow-) transitioning TC is also a smaller (larger) and weaker (stronger) TC on average

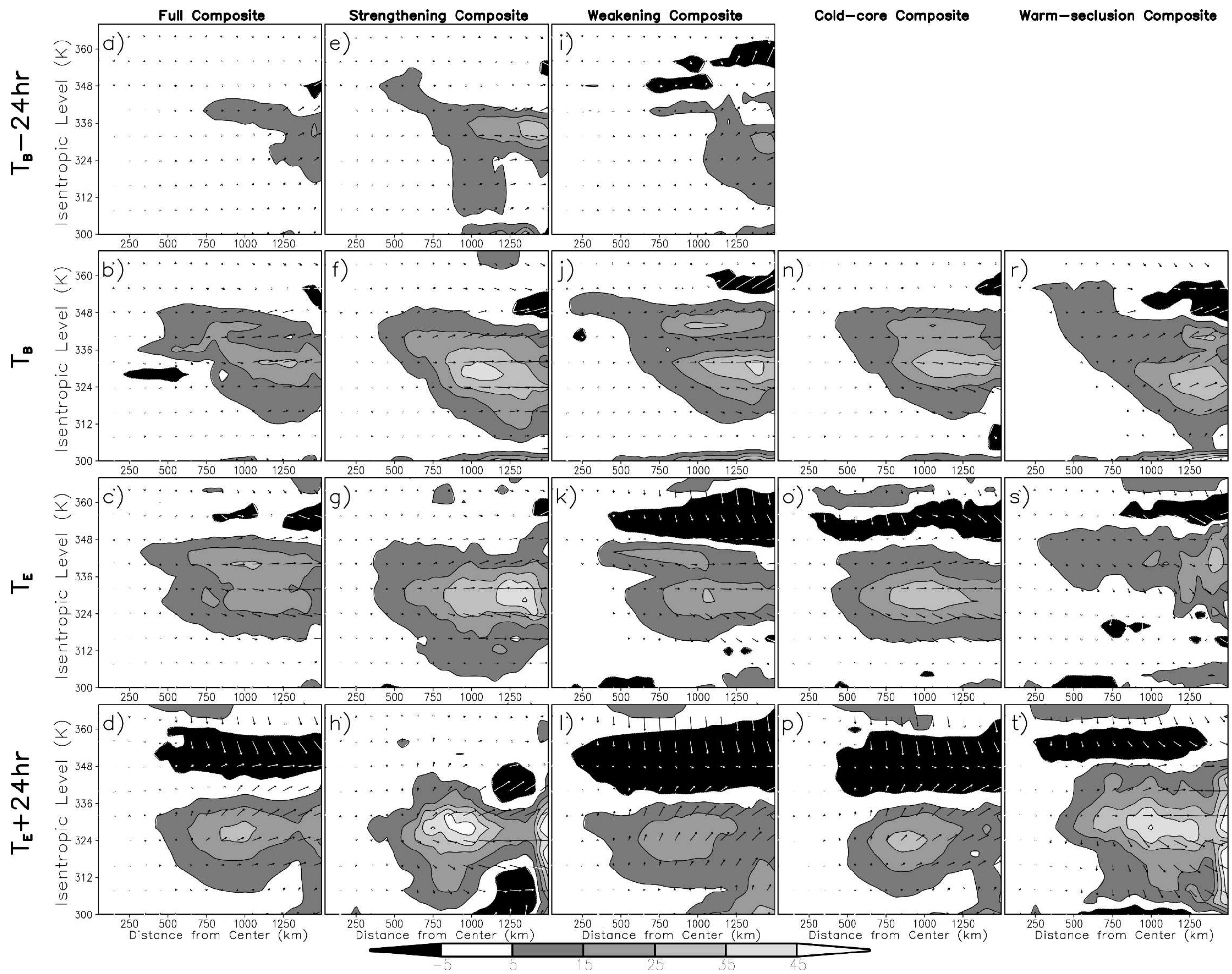

FIG. 8. Cross sections (r–θ) of Eliassen–Palm flux vectors and their divergence (shaded; 10^5 Pa m^2 K^{-1} s^{-2}) for (columns) each subcomposite at four of the key ET benchmarks: $T_B - 24$ h, T_B, T_E, and $T_E + 24$ h. Radial component of the vector is the angular momentum flux, while the vertical component is the heat flux. Outward pointing arrows represent inward eddy angular momentum flux while downward-pointing arrows represent outward eddy heat flux. Method based on Molinari et al. (1995). Subcomposite fields were not calculated for $T_B - 24$ h for the cold-core and warm-seclusion subcomposites.

(Table 3). This intensity differs by a full Saffir–Simpson category. Although requiring further study, it would seem that a smaller and weaker TC would be more prone to the shearing effects of a midlatitude trough, more rapidly removing the tropical aspects of the cyclone. It is noteworthy that there is no statistically significant difference in the mean latitude of slow- versus fast-transitioning TCs (Table 3), arguing that the statistically significant size difference at T_B (Table 3) is not due to changes in Coriolis during conservation of absolute angular momentum.

b. *Discrimination of post-ET intensification from decay*

Determination of whether a cyclone will undergo intensification or decay post-ET is critical to accurate forecasting of the storm-related weather at this stage. Post-ET intensity change is defined here as the change in minimum MSLP between T_E and $T_E + 24$ h. Intensification (decay) is defined as a 4 hPa or larger magnitude decrease (increase) in minimum MSLP in this 24-h period. Cases where the cyclone interacted with land during ET have been excluded to focus on the atmosphere pattern differences. The cases for each member are identified in Table 1, with 11 cases of weakening and 6 cases of strengthening post-ET once overland cases are excluded.

To focus on the precursor conditions leading to post-ET intensity change, subcomposites of the two groups of intensity change are produced for the time T_B (Fig. 12). The orientation of the tilt of the 500-hPa trough (Figs. 12a,b) is the most striking distinction between

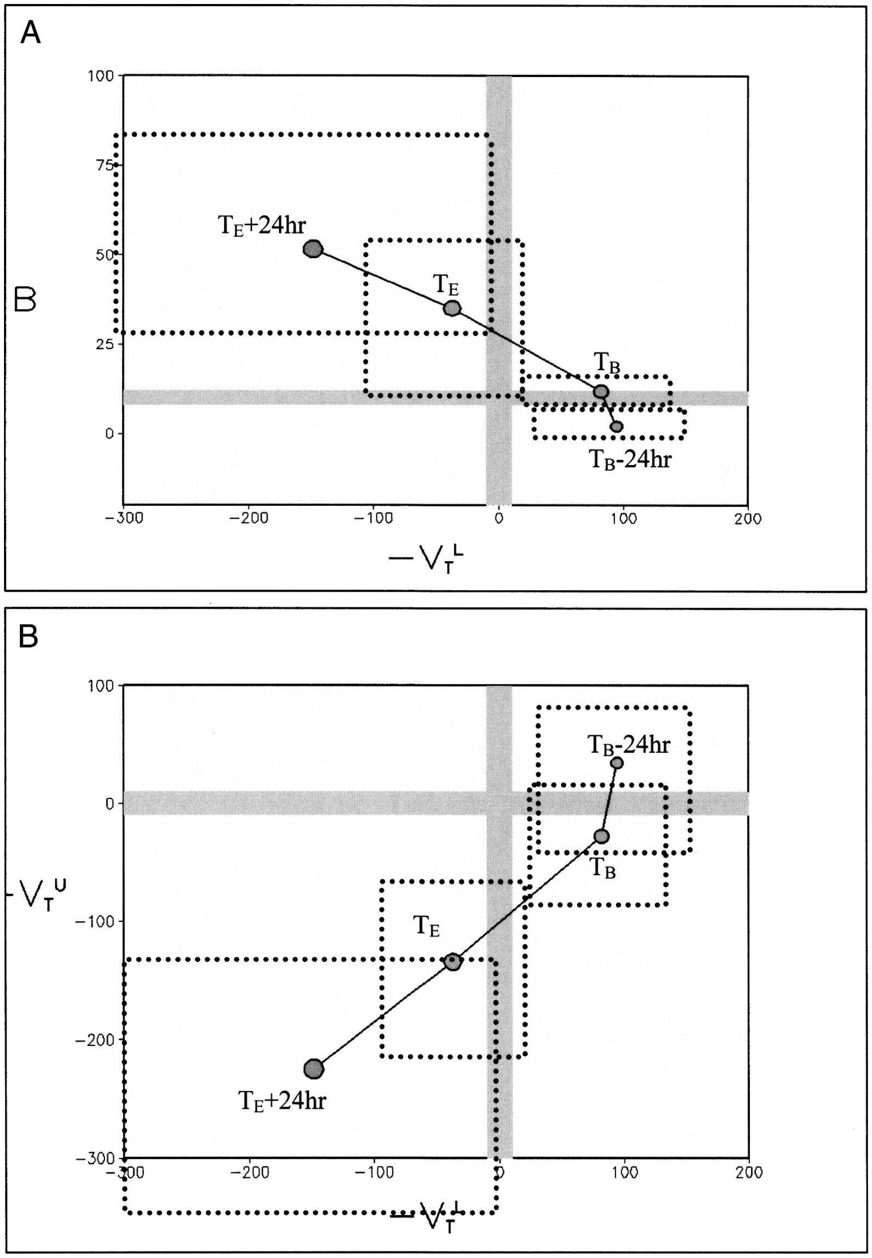

FIG. 9. One standard deviation spread about the composite mean trajectory for (a) B vs $-V_T^L$ and (b) $-V_T^L$ vs $-V_T$ at each of the four key times analyzed here: T_B − 24 h, T_B, T_E, and T_E + 24 h. Gray bars are the general division among the four cyclone phase quadrants in each figure.

these intensity subcomposites. For the post-ET intensifiers (weakeners), a negatively (positively) tilted 500-hPa large-scale trough is advancing on the TC. Also noteworthy is that the separation distance between the trough and TC varies considerably between the composites, with the post-ET intensifier having a much closer approach than the post-ET weakener. However, the number of cases in this sample (six) strongly argues for further investigation of this sensitivity, and statistical significance of these results are discussed in section 4d. Indeed, two such cases preceding this study [Iris (1995) and Lili (1996)] do not conform to this result (Thorncroft and Jones 2000). A post-ET intensifying cyclone has an associated maximum of 850-hPa equivalent potential temperature that extends 10° equatorward, while the post-ET weakeners are far more isolated from the tropical environment (Figs. 12c,d). SSTs below an intensifying storm are 1°–2°C higher than be-

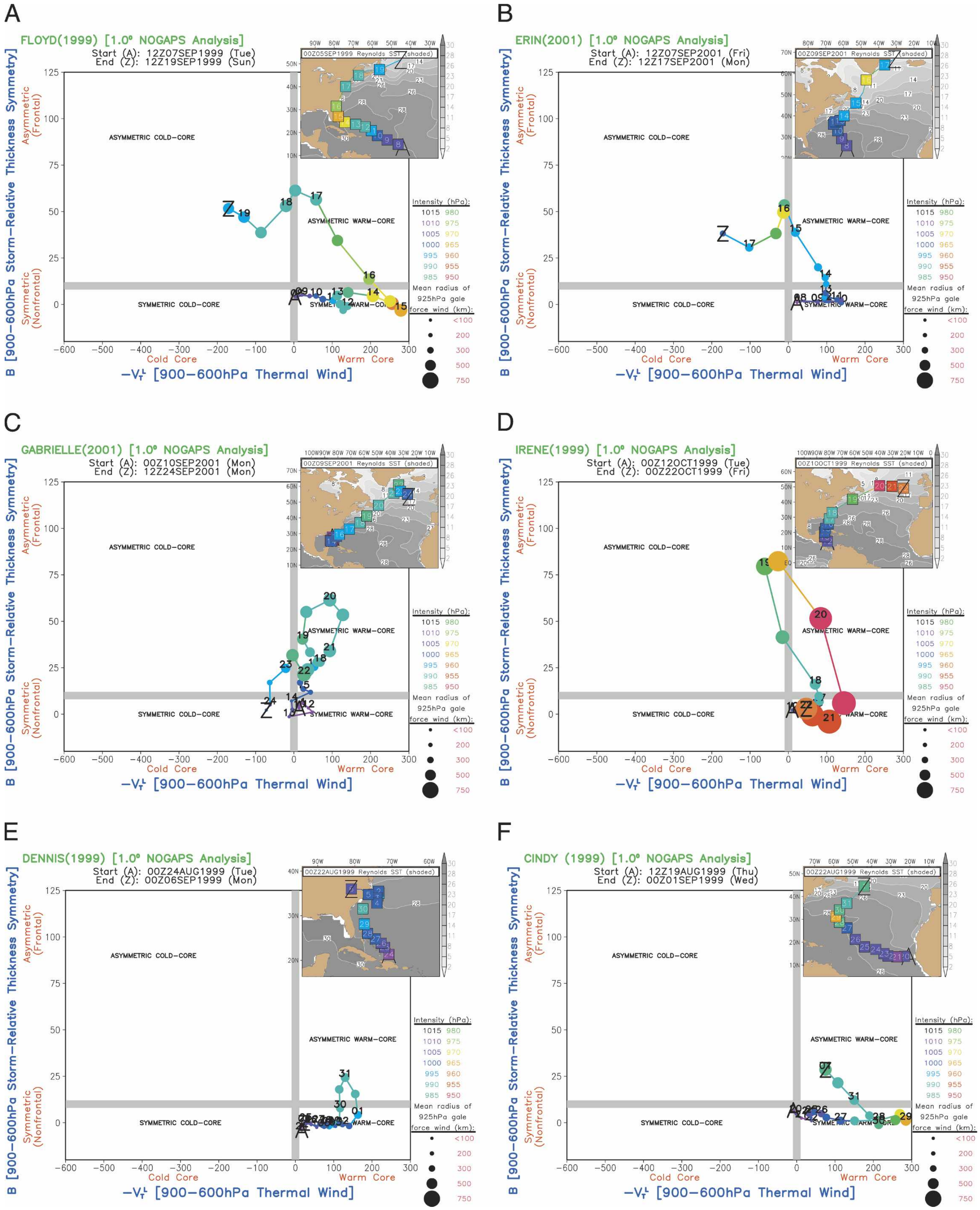

FIG. 10. Examples of the variety of posttransition structural evolutions comprising the 34-member ensemble that lead to the dramatic increase in post-ET variability shown in Fig. 9: (a) Cold-core decay [Floyd (1999)]. (b) Cold-core intensification [Erin (2001)]. (c) Extended hybrid existence [Gabrielle (2001)]. (d) Warm-seclusion development [Irene (1999)]. (e) Halted ET and reacquired tropical structure [Dennis (1999)]. (f) Absorption by preexisting cyclone [Cindy (1999)]. Only two dimensions (B vs $-V_T^L$) of the cyclone phase space are shown.

TABLE 3. Mean statistics on each of the composites. Standard deviation is denoted in parentheses. Statistically significant departures within each subcomposite (slow vs fast, intensifier vs weakener, and warm seclusion vs cold core) to 90% (95%) confidence using a *t* test, are in italic (bold italic). Note that the subcomposites are not independent. Thus a single storm may contribute, e.g., to the post-ET intensifier, *and* the warm-seclusion subcomposites.

	No. of cases	Mean latitude at T_B	Mean longitude at T_B	Mean NHC best-track intensity at T_B (hPa)	Mean NHC mean radius of gale-force winds at T_B (km)
Entire composite	34	34.3 (5.8)	−65.6 (16.1)	982.8 (15.3)	211.8 (97.4)
Slow-transitioning TC subcomposite	9	33.0 (6.2)	−66.5 (14.4)	***972.8*** (***16.2***)	*263.0* (*59.7*)
Fast-transitioning TC subcomposite	10	36.1 (5.0)	−67.2 (11.4)	***987.7*** (***13.9***)	*184.3* (*115.8*)
Post-ET intensifier subcomposite	6	37.0 (1.8)	−59.8 (7.3)	980.6 (15.1)	255.3 (107.2)
Post-ET weakener subcomposite	11	36.2 (4.9)	−63.0 (15.8)	982.6 (11.5)	194.2 (90.2)
Post-ET warm-seclusion subcomposite	6	32.5 (6.7)	*−72.7* (*15.5*)	982.0 (13.5)	***259.8*** (***64.0***)
Post-ET cold-core subcomposite	15	36.2 (4.6)	*−57.9* (*15.2*)	986.5 (13.2)	***171.1*** (***96.6***)

low a weakening storm, but there is also a substantially increased gradient of SST below a strengthening storm. These results are all consistent with the idealized models favoring baroclinic growth (Charney 1947; Eady 1949) and reinforce the conclusion that the basic structure of both the TC and midlatitude trough play key roles in determining the nature of posttransition intensity change.

An even more striking comparison of the evolutions leading to post-ET weakening versus strengthening can be found in the time sequence of EP flux divergence for the mean atmosphere of the two subcomposites (Figs. 8e–l). The post-ET strengthening subcomposite (which has a negatively tilted trough driving it; Fig. 12b) is associated with significantly stronger eddy PV flux (from primarily inward transport of eddy angular momentum) at smaller radii than the post-ET weakening subcomposite (Figs. 8i–l). The weakening subcomposite shows a maximum of eddy PV flux that contracts until T_E, after which it weakens and becomes less distinct. In contrast, the strengthening composite eddy PV flux undergoes a significant contraction and intensification between T_E and T_E + 24 h. This dramatic enhancement and contraction of the eddy PV flux maximum is made possible by the negative tilt of the synoptic-scale trough. The negative trough tilt both permits the TC to approach the trough to a much smaller distance, and also drives heat and momentum fluxes that amplify the trough itself (Bluestein 1992, 1993), further increasing the eddy PV flux into the cyclone (Figs. 8g,h).

c. *Posttransition warm seclusion from cold-core evolution*

Shapiro and Keyser (1990) documented an extension to the fundamental cold-core life cycle of extratropical cyclones. The development of a warm seclusion within the center of extratropical cyclones can be achieved either as a precursor to, or as a result of, rapid intensification of extratropical cyclones (Hart 2003). An example of such a warm seclusion is shown in Fig. 13, with the ET and warm seclusion of Hurricane Danielle (1998). While the CPS evolution of Danielle begins as a typical ET (Fig. 13a), instead of undergoing cold-core development the post-ET evolution is that of increasingly symmetric, warm-core development (Fig. 13b). The warm core is typically restricted below 600 hPa (Hart 2003), distinguishing the warm-seclusion development from the deep warm-core development of TCs. Another distinctive factor is the dramatic expansion of gale-force winds associated with warm seclusions (Figs. 13e,f). During a warm seclusion, the strongest winds contract in radius while the radius of gale-force winds expands. Thus, the development of a warm seclusion represents a dramatic increase in wind-driven threat through increases in both the area and magnitude of ocean-wave growth and land surface damage potential. Essentially, the warm-seclusion process of an extratropical cyclone results in the combined threats of a cold-core cyclone (expanded area of strong winds) and TC (increased upper bound of destructive wind magni-

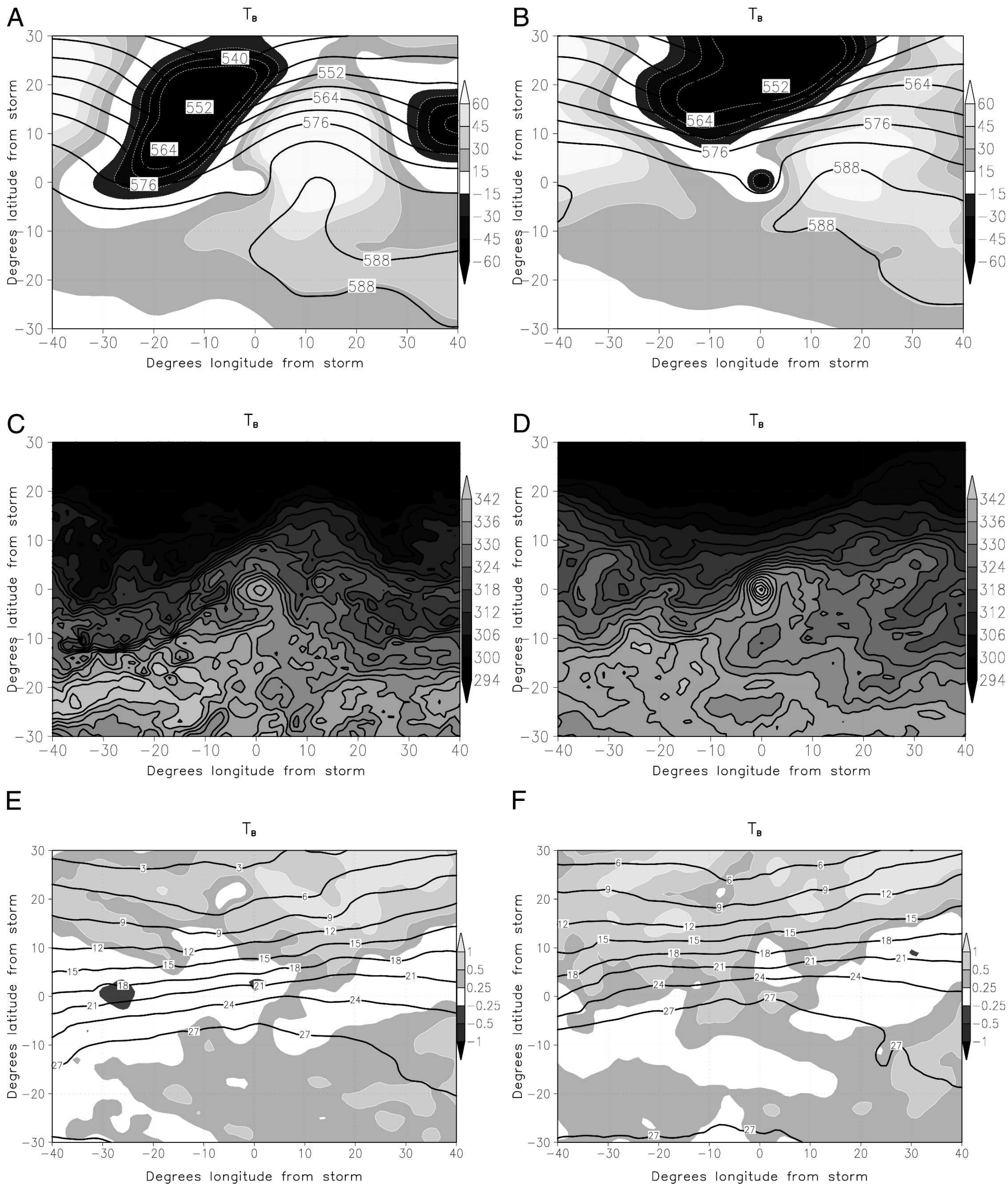

FIG. 11. Comparison of the environments at T_B of cyclones that take (left) 12 h or less and (right) 48 h or more to complete transition (Table 1): (a), (b) 500-hPa height (contour, dm) and anomaly from monthly mean (shaded, m); (c), (d) 850-hPa equivalent potential temperature; and (e), (f) SST (contour, °C) and anomaly from 1990 to 2003 weekly mean (shaded, °C).

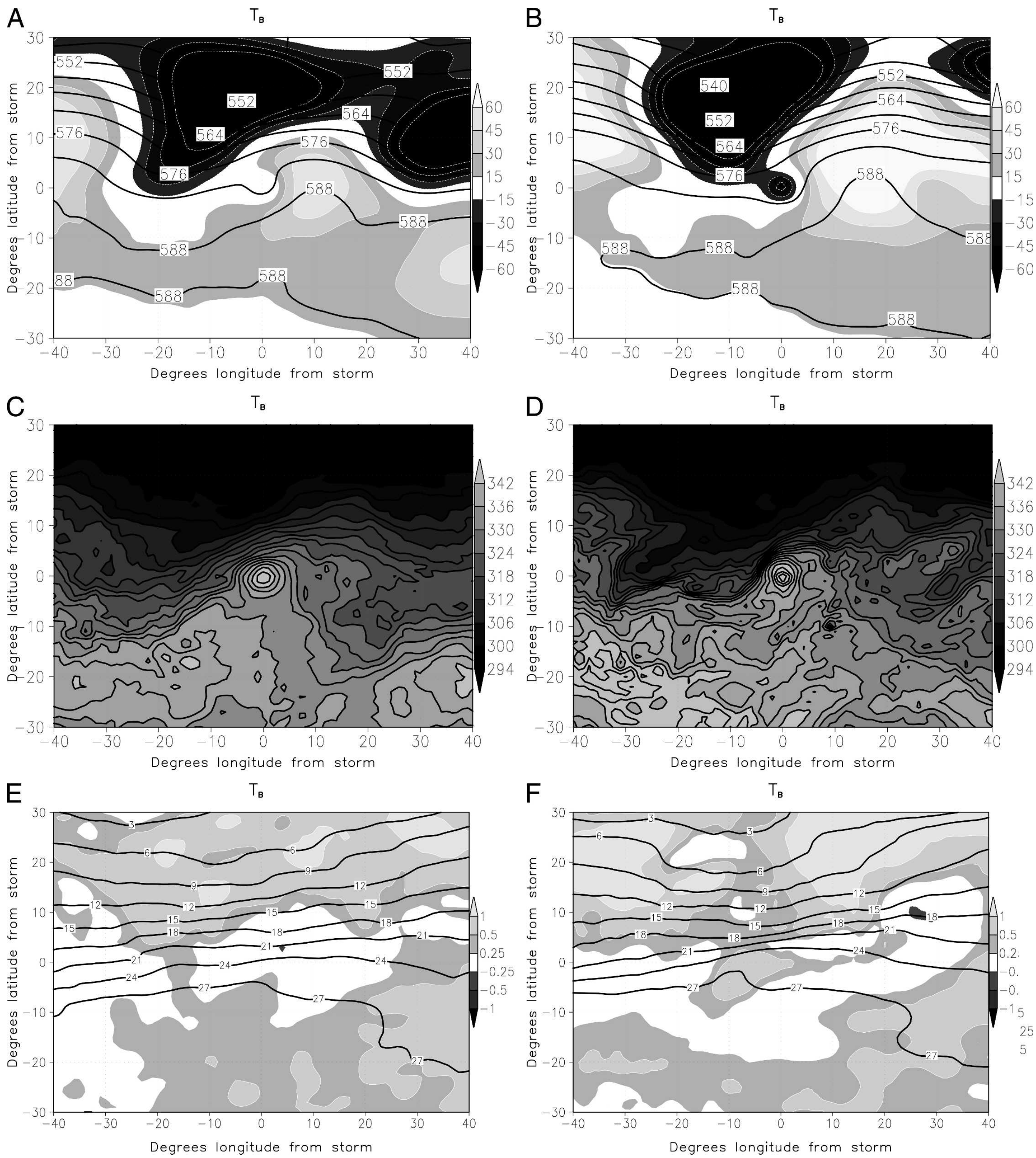

FIG. 12. The T_B subcomposites for post-ET: (left) weakening or (right) strengthening. Weakening (strengthening) storms increase (decrease) in MSLP by at least 4 hPa between T_E and T_E + 24 h: (a), (b) 500-hPa height (contour) and anomaly from zonal mean (shaded); (c), (d) 850-hPa equivalent potential temperature (shaded); (e), (f) SST (°C) and anomaly (°C) from 1990 to 2003 weekly mean.

tude). As this type of development is often difficult to forecast numerically because of sensitivity to heating magnitude and distribution (Gyakum 1983a,b), it is critical to understand the precursor conditions that distinguish a future warm seclusion from a conventional cold-core post-ET evolution (Fig. 14). As not all warm seclusions intensify (McTaggart-Cowan et al. 2001, 2003; Table 1), it is equally important to diagnose

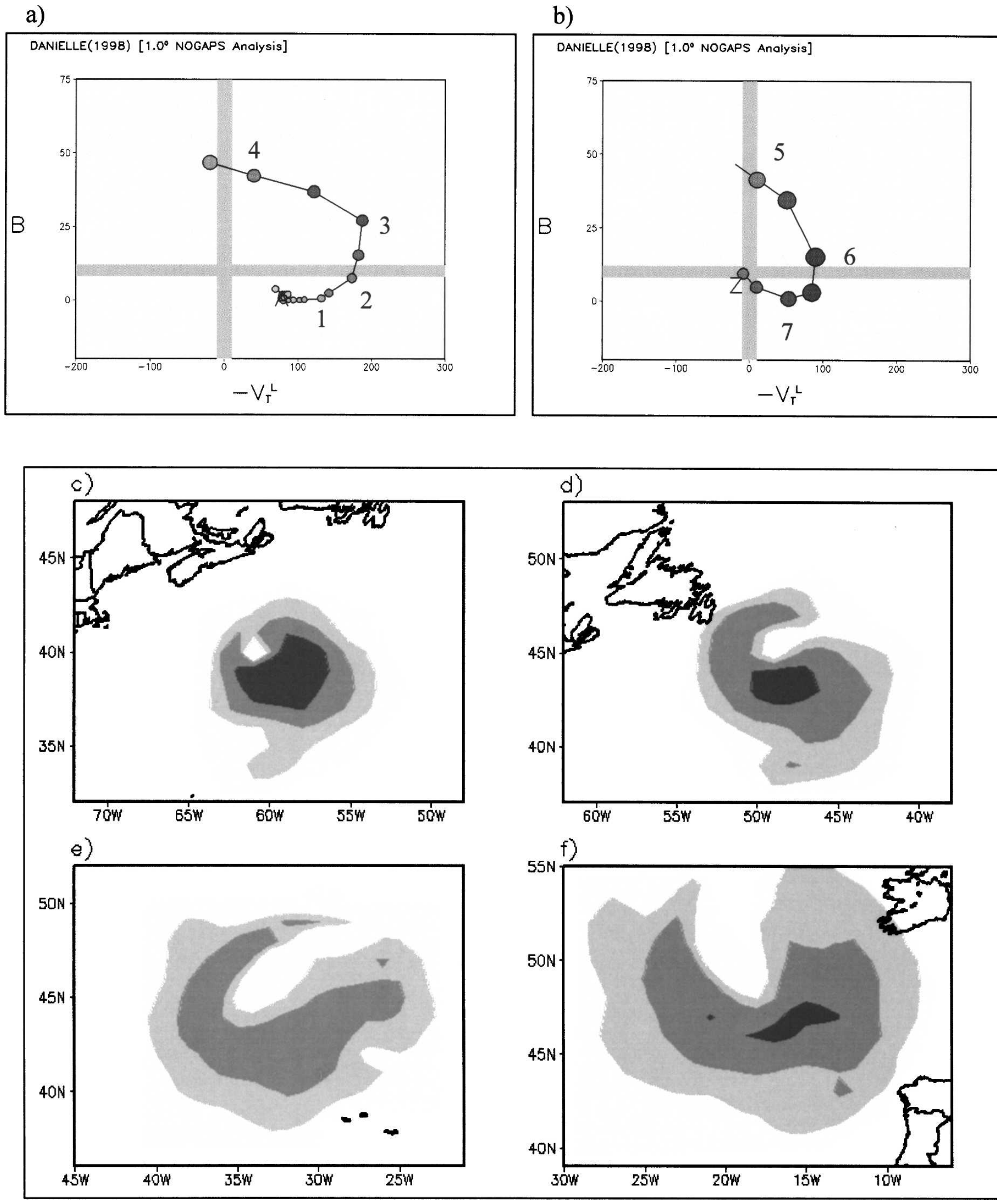

FIG. 13. Analysis of the ET and warm seclusion of Hurricane Danielle (1998): (a) B vs $-V_T^L$ cyclone phase space analysis, with a zoomed domain. The first half of the life cycle is shown here, from tropical development, maturity, to ET. (b) The second half of the Danielle life cycle, including warm seclusion and then occlusion. The day (5 = 5 Aug 1998) has been labeled for the 0000 UTC positions. (c)–(f) Distribution of 925-hPa wind field for gale, storm, and hurricane threshold wind on 0000 UTC 3–6 Sep 1998, respectively.

whether the warm seclusion is a *response* to the intensification, or the *cause* of it.

The process of warm seclusion is a classic case of scale matching, aided by a narrowing of the approaching trough as in Molinari et al. (1995). As evidenced by the 500-hPa analysis (Figs. 14a,b) and the isentropic potential vorticity (Figs. 14c–f), the scale of the midlatitude trough is key to determining the structural evolution of the cyclone after T_E. Cyclones that undergo a warm seclusion after T_E interact with a trough that is considerably narrower in horizontal scale, but more extensive in vertical scale, than a cyclone that remains cold core after T_E. Thus, for a future warm seclusion the horizontal and vertical scale of the trough is a closer match to that of the tropical storm (Fig. 14c versus 14d) and the trough signature itself also extends much lower

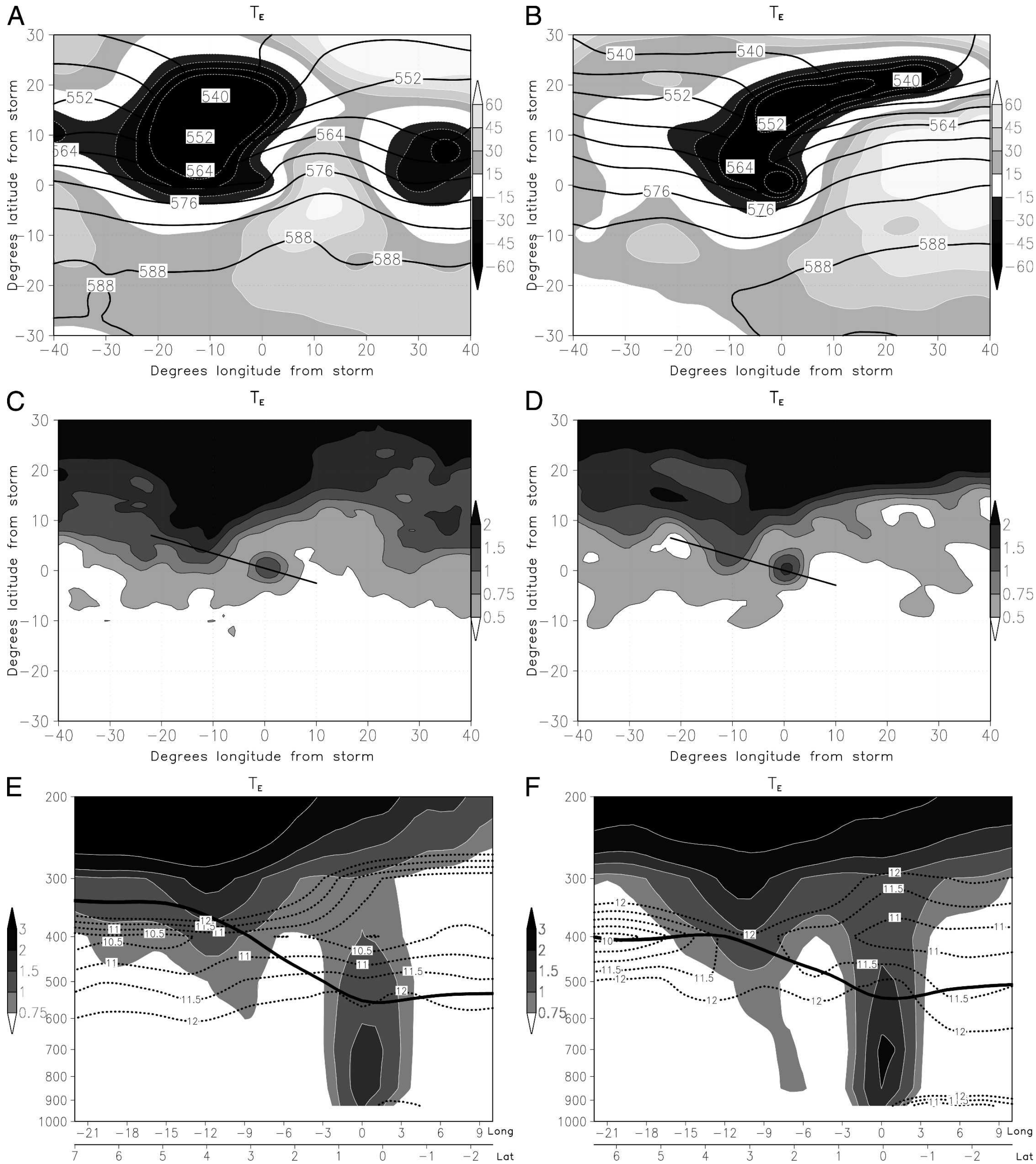

FIG. 14. Synoptic environments at T_E that lead to (left) cold-core evolution and (right) warm-seclusion evolution after T_E: (a), (b) 500-hPa height (contour, dm) and anomaly from monthly mean (shaded, m); (c), (d) 320-K isentropic potential vorticity (shaded, PVU); (e), (f) potential vorticity cross section along axis shown in (c), (d); (g), (h) 850-hPa equivalent potential temperature (shaded); (i), (j) Reynolds weekly averaged sea surface temperature (contour, °C) and anomaly from 1990 to 2003 weekly mean (shaded, °C).

into the troposphere (Fig. 14e versus 14f) than for a post-ET cold-core development, consistent with Molinari et al. (1995) and Hanley et al. (2001). Indeed, a TC that undergoes a warm seclusion is on average 50% larger than a TC that remains cold core after transition (Table 3). Thus, the scale matching is achieved through an above-average TC size along with a narrowing of the trough.

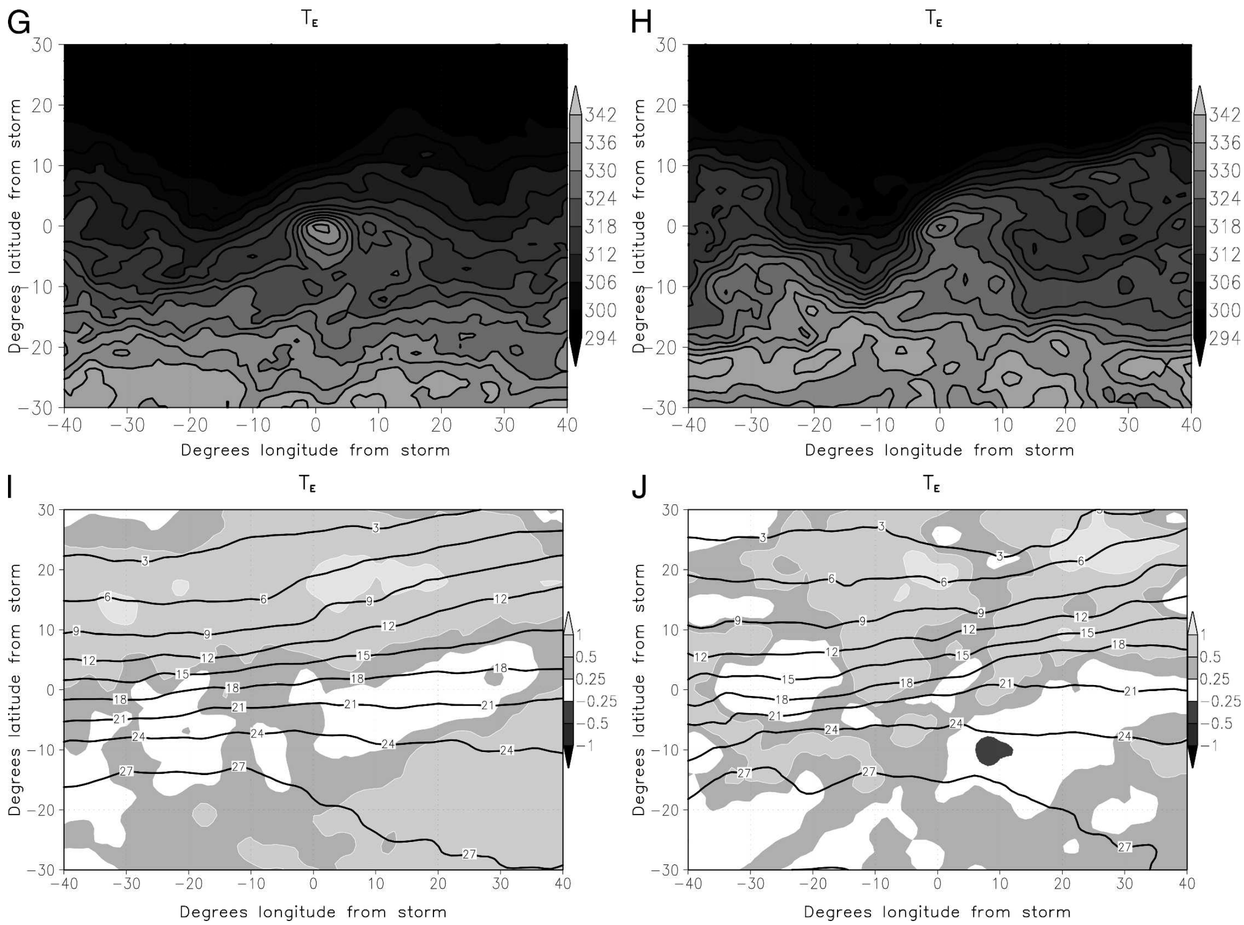

FIG. 14. (*Continued*)

As was the case in the previous subcomposite intercomparison, the Eliassen–Palm flux vector comparisons for the cold-core versus warm-seclusion subcomposites are insightful for explaining the details and sensitivity of the interaction (Figs. 8n–t). In particular, while the cold-core composite is unremarkable, at the end of transition (Fig. 8o), the warm-seclusion subcomposite bears considerable resemblance to the trough interaction case of Elena (Fig. 8s; cf. with Molinari et al. 1995, their Figs. 3c, d). While all other cross sections in Fig. 8 show a level of maximum eddy PV flux below 330 K, Fig. 8s alone has a level of maximum PV flux of 340–345 K, approximately the same as for Elena (1985). As Molinari et al. (1995) argued in the case of Elena, the narrowing of the trough as it approaches the TC leads to eddy angular momentum flux that is focused on the outflow anticyclone of the TC (due to Rossby depth reduction). The (in)direct circulation (above) below 345 K regains thermal wind balance through adiabatic motion. As a response to this motion, the secondary circulation of the TC is enhanced and there is a short-term intensification. This begs the question, then, of how the cyclone response is different if the cyclone is transitioning to cold core.

Figure 8r suggests that the start of transition for a future warm seclusion is not unique. There is a deep layer of eddy PV flux that is maximized in the middle troposphere (325 K). The cyclone responds to this forcing as described in section 3b. Based upon Fig. 8r, it would appear that the scale of the trough does not play a factor while the trough is still beyond the extreme outer edge of the TC circulation (Fig. 14d). However, instead of continuing to deepen and strengthen as was the case in the other subcomposites (Figs. 8c,g,k,o), the region of eddy PV flux suddenly contracts and moves upward—in response to the narrowing of the trough (Figs. 14d,f). Thus, in the middle of transition, the TC is now in an environment for an Elena-type rapid intensification. With the sudden scale decrease and elevation of the eddy PV flux, a much more focused eddy momentum response occurs, as did with Elena (Molinari et al. 1995). A direct (enhanced secondary) circulation forms within the entire troposphere below 345 K, causing dramatically enhanced low-level inflow, adiabatic ascent at inner radii, and outflow at the 345-K level, to restore thermal wind balance. The cyclone response as a consequence of this eddy-forcing change during transition is seemingly the generation of a warm seclusion around or after T_E + 24 h. The details of how this dramatic change in eddy momentum forcing leads to a warm seclusion instead of cold core require numerical simulation, and is being pursued (Maue and Hart 2005).

One day following transition, this rapid contraction is illustrated in Fig. 8t, with the deepest layer of inward eddy PV flux of any of the panels on Fig. 8. The deep layer of downward EP flux vector in Fig. 8t is indicative of the formation of the warm seclusion, since the vector direction indicates intense heat flux outward from the center of the vertically upright lower-tropospheric vortex. Finally, it is worthwhile to note that there are no significant differences in the SST field (Fig. 14i,j) beneath the cyclone that becomes a warm seclusion and the cyclone that remains cold core.

d. Subcomposite statistical significance

While the results of the composites are often strikingly different subjectively, given the relatively low number of members in each composite (varying from 6 to 11), the statistical significance of these differences needs to be quantified. The statistical significance of the difference in the means among the various subcomposites (slow- versus fast-transitioning TC, weaken versus intensify post-ET, and warm-seclusion versus cold-core post-ET structure) was calculated using a Student's *t* test (Fig. 15). The analysis illustrates that there is moderate to strong statistical significance in the key features previously argued to be responsible for distinguishing the post-ET evolutions.

For the distinction of slow versus fast transition (Fig. 15a), the upstream and downstream 500-hPa trough/ridge pattern (determining the steering of the TC with respect to the SST gradient) is statistically significant to 95% and 90% confidence, respectively. For the weakening versus strengthening subcomposites (Fig. 15b), there is 90%–95% confidence in the key features at 500 hPa: TC intensity and upstream trough tilt. For the factors distinguishing cold-core versus warm-seclusion post-ET evolution (Figs. 15c,d), we find a similar result. At 500 hPa, the downstream ridge/trough pattern is significant to 95%–99% confidence (Fig. 15c), illustrating the strong role the downstream ridge plays in narrowing the scale of the upstream trough. However, the upstream trough itself is significant only to 75% confidence. Given that the distinction for cold-core versus warm-seclusion evolution is largely the scale of the trough both horizontally and vertically (section 4d), 500 hPa is not an ideal level to examine for significance.

If we examine the statistical significance of the PV differences in Fig. 14e versus Fig. 14f, we can visualize the statistically significant areas more clearly (Fig. 15d). The TC structure itself is statistically significant to 95% confidence, with the greatest significance around 400–500 hPa. There is also high statistical significance (90%–95%) in both the magnitude of the upstream trough at 200–250 hPa, but also in the amplitude of the trough (as represented by the 400-hPa region upstream). These two regions combined illustrate that the scale of the upstream trough indeed plays a statistically significant role in determining whether scale matching occurs and, thus, the post-ET evolution: cold core or warm seclusion. It is worthwhile to note that the near-surface extension (to $-6°$ longitude/2.5° latitude upstream of the TC) of the upstream trough is statistically significant to 75% confidence. While the maps of statistical significance shown in Fig. 15 give strong support for the factors driving post-ET evolution discussed previously, many more cases are needed to further refine this analysis and to illuminate post-ET structural evolutions that have not yet been analyzed [e.g., warm-seclusion strengtheners versus warm-seclusion weakeners; differences between ET over land (ignored here) versus over water].

5. Summary and concluding remarks

The evolution of a TC from a warm-core vortex to a cold-core vortex is largely driven by the eddy angular momentum flux of the trough, rather than the eddy heat flux associated with the trough. The response of the transitioning cyclone to the tropospheric-deep PV forcing is to produce adiabatic ascent and cooling inward and beneath the region of the eddy forcing to restore thermal wind balance. In the case of ET, the eddy PV flux forcing is maximized considerably lower in the atmosphere, and spread over much greater depth, than in the case of rapid intensification of a hurricane [e.g., Elena (1985); Molinari et al. 1995]. Only after ET has completed (T_E in the cyclone phase space) is the eddy heat flux forcing diagnosed as significant (e.g., Figs. 8d,l,p,t), consistent with Harr et al. (2000).

While roughly 50% of North Atlantic TCs undergo ET, the structural evolutions of the post-ET cyclones vary greatly, as does their intensity change following transition. As demonstrated here, the nature of the ET evolution and intensity change is sensitive to the scales of interaction of the trough and TC, in both space and time. The tilt and scale of the interacting trough play statistically significant roles throughout the entire evo-

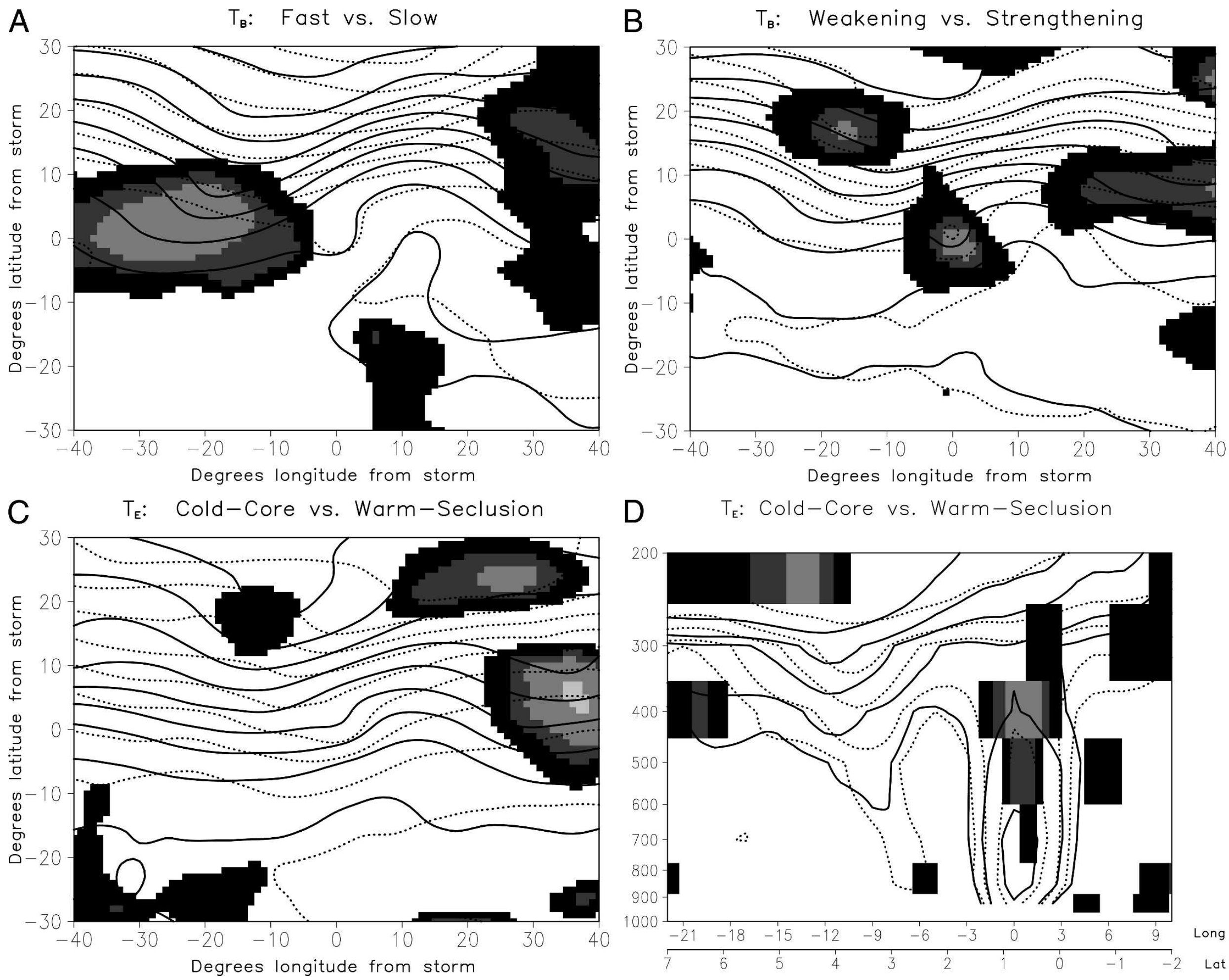

FIG. 15. Statistical significance (Student's *t* test) of the difference among the means of the various subcomposites: (a) 500-hPa height for fast ($n = 10$) vs slow ($n = 9$) transitioning; (b) 500-hPa height for weakening ($n = 11$) vs strengthening ($n = 6$) after T_E; (c) 500-hPa height for cold core ($n = 15$) vs warm seclusion ($n = 6$) after T_E + 24 h; (d) PV cross section shown in Figs. 15e,f for cold core vs warm seclusion. Regions of statistically significant difference are shaded. The four shades are 75%, 90%, 95%, and 99% confidence. The solid contour is the first listed field in the title and the dotted contour is the second.

lution, while the SST appears to play an important role only until transition is completed. A TC undergoes rapid ET if the long-wave pattern is highly meridional, the SST are several degrees below 27°C with a large SST gradient, and the TC is significantly smaller and weaker than average at the beginning of ET (Table 3). A TC undergoes slow transition (and has an extended hybrid phase) if the long-wave pattern is more zonal, the SST beneath the TC are closer to 27°C, and the TC is significantly larger and stronger than average; this combination of environmental forcings continues to support tropical development (SST ~ 27°C) at the same time as ET is occurring.

Once transition completes (T_E), an ET–TC will undergo posttransition intensification if the interacting trough is negatively tilted and the remnant TC is intense. If the remnant TC is weak or the interacting trough is positively tilted, the ET–TC will weaken. In the 24–48 h following transition, approximately 70% of ET cases result in cold-core evolutions while 30% result in warm seclusions. If the interacting trough acquires a size that permits scale matching with the remnant TC (minimizes the trough scale), then a warm seclusion (cold-core cyclone) results. A warm seclusion occurs as a consequence of the eddy PV flux from the trough contracting to the outflow layer of the transitioning TC, consistent with the Molinari et al. (1995) model for Elena (1985).

Of the 30% (6/21) of cyclones that become warm seclusions, 4/6 rapidly intensify during the seclusion while 2/6 weaken. This intensity change during warm seclusion may be dependent on the timing of the TC–

trough interaction, although there are not yet enough cases to clearly distinguish this. As warm seclusions represent the combined threats of tropical and extratropical cyclones, accurate prediction of this evolution is key to the protection of life and property at middle to high latitudes.

The results presented here suggest sources of the abnormally low predictability of the long-wave pattern during ET events. Differences in TC intensity, depth, trough tilt or scale, or latitude of transition (SST) can lead to extreme variability in the forecast evolution of the post-ET cyclone *and* the interacting long-wave pattern. With numerical models initializing TCs often 30–50 mb too weak, it is not at all surprising to find the great disparity of ET structural forecasts today (http://moe.met.fsu.edu/cyclonephase; Hart and Evans 2003; Evans and Arnott 2004). The results of this research argue that great care must be taken when initializing numerical models around the time of an ET event. Models that initialize TCs too strongly warm core or too large at higher latitudes would lead to overprediction of warm seclusions, while models that initialize TCs too weakly or too small at higher latitudes would lead to overprediction of decaying cold-core systems. Thus, it is important to understand how well the evolving tropical storm structure is initialized in the operational models, including the use of synthetic observations (Goerss and Jeffries 1994; Kurihara et al. 1998; Liu et al. 2000). This sensitivity to model initialization is the subject of current research (e.g., Evans and Arnott 2004).

In addition to the tropical vortex, all of these evolutions depend upon the scale and timing of the interacting trough, which also may not be sufficiently well analyzed, especially over the oceans. Thus, improved analysis of areas producing sensitivity to ET and post-ET track and intensity forecasts should be a priority to improve midlatitude forecasts (Jones et al. 2003b). Further, with 3–5-day official track forecast errors by the National Hurricane Center (NHC) averaging 300–500 km (and recurving storms having even larger errors on average), one can readily see how even average track forecast error in a numerical forecast can lead to a dramatic change in the simulated TC–trough interaction and thus post-ET evolution.

6. Future work

A more detailed examination of the distinctions among the subcomposites using a larger database size is ongoing. Although the statistics shown here are significant, a larger case size would add further confidence and may illuminate additional important precursor differences. Although all the cases of ET studied here had an upper-level trough within 1500 km, a larger database size may reveal that there are cases of ET where only low-level temperature gradients can produce ET (e.g., a strong SST gradient without an atmospheric trough; Sekioka 1957).

The relationship among the various subcomposites should be studied using a larger database, to produce a more cohesive picture of the nature of ET evolution and precursor conditions. For example, the distinction among whether the warm seclusion is the cause of, or is caused by, rapid intensification has yet to be determined. Numerical modeling is needed to examine the details of the trough interaction in the warm-seclusion process. In particular, how the timing of the trough narrowing during ET (Fig. 8) plays so crucial a role in the development of the warm seclusion instead of the cold-core evolution.

Although the performance of numerical models at forecasting ET has been examined to some degree (Jones et al. 2003b; Ma et al. 2003; Evans and Arnott 2004), a more vigorous study of the forecast skill among each of the subcomposite evolutions should be performed. Such a study would help determine the sources for numerical prediction uncertainty and identify more clearly the forecast situations where numerical models are prone for large forecast error. During times of ET events, forecast predictability could be aided by including larger perturbations in the trough/TC intensity and scale to determine the sensitivity of the initialized model evolution to the details of scale interaction. The dynamics of wind field expansion by ET cyclones, despite having immense practical value, remains largely unexplored territory although it is actively being pursued (Evans and Hart 2005).

Acknowledgments. The first author was funded by a UCAR visiting scientist position during the early part of this research and is grateful to UCAR, NCEP, and in particular Steve Lord and Naomi Surgi of NCEP/EMC for making this support possible. The first author was also funded by a Florida State University CRC FYAP grant during the second half of this research. The second author was supported by the National Science Foundation under Grant ATM-0351926. The third author was supported by an AMS/ONR Fellowship. The authors are grateful to these organizations for their support.

The NOGAPS analysis and forecast data were provided by Mike Fiorino of Lawrence Livermore National Laboratory. Figures for this paper were created using the GrADS software package from COLA/IGES. The research has greatly benefited from discussions with Eyad Attalah of McGill University, Lance Bosart of SUNY Albany, and Ryan N. Maue of Florida State University. The authors also appreciate the constructive feedback of four anonymous reviewers.

REFERENCES

Agusti-Panareda, A., C. D. Thorncroft, G. C. Craig, and S. L. Gray, 2004: The extratropical transition of Hurricane Irene (1999): A potential vorticity perspective. *Quart. J. Roy. Meteor. Soc.,* **130,** 1047–1074.

Arnott, J. M., J. L. Evans, and F. Chiaromonte, 2004: Characterization of ET using cluster analysis. *Mon. Wea. Rev.,* **132,** 2916–2937.

Bluestein, H. B., 1992: *Kinematics and Dynamics.* Vol. I, *Synoptic-Dynamic Meteorology in the Mid-Latitudes,* Oxford University Press, 431 pp.

——, 1993: *Observations and Theory of Weather Systems.* Vol. II, *Synoptic-Dynamic Meteorology in the Mid-Latitudes,* Oxford University Press, 594 pp.

Bosart, L. F., E. H. Atallah, and J. E. Molinari, 2001: The quantitative precipitation forecast problem associated with landfalling and transitioning tropical cyclones. Preprints, *Symp. on Precipitation Extremes,* Albuquerque, NM, Amer. Meteor. Soc., 359–362.

Bowyer, P. J., 2000: Phenomenal waves with a transitioning tropical cyclone (Luis, the Queen, and the buoys). Preprints, *24th Conf. on Hurricanes and Tropical Meteorology*, Fort Lauderdale, FL, Amer. Meteor. Soc., 294–295.

——, and C. Fogarty, 2003: Hurricane Juan: A forecasting perspective. *Proc. Second Int. Workshop on ET*, Halifax, NS, Canada.

Brand, S., and C. P. Guard, 1978: Extratropical storm evolution from tropical cyclones in the western North Pacific Ocean. Naval Environmental Prediction Tech. Rep. TR78-02, 20 pp.

Caplan, P., J. Derber, W. Gemmill, S.-Y. Hong, H.-L. Pan, and D. Parrish, 1997: Changes to the 1995 NCEP Operational Medium-Range Forecast Model Analysis–Forecast System. *Wea. Forecasting,* **12,** 581–594.

Charney, J. G., 1947: The dynamics of long waves in a baroclinic westerly current. *J. Meteor.,* **4,** 135–162.

Eady, E. T., 1949: Long waves and cyclone waves. *Tellus,* **1,** 33–52.

Elsberry, R. L., Ed., 1995: Global perspectives on tropical cyclones. WMO Rep. TD-No. 693, Geneva, Switzerland, 289 pp.

Evans, A. C., and R. E. Hart, 2005: Towards a better understanding of and ability to forecast the wind field expansion during the extratropical transition process. Preprints, *21st Conf. on Weather Analysis and Forecasting*, Washington, DC, Amer. Meteor. Soc., CD-ROM, P1.17.

Evans, J. L., and R. E. Hart, 2003: Objective indicators of the onset and completion of ET for Atlantic tropical cyclones. *Mon. Wea. Rev.,* **131,** 909–925.

——, and J. M. Arnott, 2004: Analysis of operational model forecast trends in ET storm structure. Preprints, *26th Tropical Meteorology and Tropical Cyclones Conf.*, Miami Beach, FL, Amer. Meteor. Soc., CD-ROM, 2C.5a.

——, and B. Prater-Mayes, 2004: Factors affecting the posttransition intensification of Hurricane Irene (1999). *Mon. Wea. Rev.,* **132,** 1355–1368.

Foley, G. R., and B. N. Hanstrum, 1994: The capture of tropical cyclones by cold fronts off the west coast of Australia. *Wea. Forecasting,* **9,** 577–592.

Goerss, J. S., and R. A. Jeffries, 1994: Assimilation of synthetic tropical cyclone observations into the Navy Operational Global Atmospheric Prediction System. *Wea. Forecasting,* **9,** 557–576.

Gyakum, J. R., 1983a: On the evolution of the *QE II* storm. Part I: Synoptic aspects. *Mon. Wea. Rev.,* **111,** 1137–1155.

——, 1983b: On the evolution of the *QE II* storm. Part II: Dynamic and thermodynamic structure. *Mon. Wea. Rev.,* **111,** 1156–1173.

Hanley, D., J. Molinari, and D. Keyser, 2001: A composite study of the interactions between tropical cyclones and upper-tropospheric troughs. *Mon. Wea. Rev.,* **129,** 2570–2584.

Harr, P., and R. L. Elsberry, 2000: ET of tropical cyclones over the western North Pacific. Part I: Evolution of structural characteristics during the transition process. *Mon. Wea. Rev.,* **128,** 2613–2633.

——, ——, and T. Hogan, 2000: ET of tropical cyclones over the western North Pacific. Part II: The impact of midlatitude circulation characteristics. *Mon. Wea. Rev.,* **128,** 2634–2653.

Hart, R. E., 2003: A cyclone phase space derived from thermal wind and thermal asymmetry. *Mon. Wea. Rev.,* **131,** 585–616.

——, and J. L. Evans, 2001: A climatology of the extratropical transition of Atlantic tropical cyclones. *J. Climate,* **14,** 546–564.

——, and ——, 2003: Analyzing and forecasting cyclone structural transition using cyclone phase diagrams. *Proc. Second Int. Workshop on ET,* Halifax, NS, Canada.

Hogan, T. F., and T. E. Rosmond, 1991: The description of the Navy Operational Global Atmospheric Prediction System's spectral forecast model. *Mon. Wea. Rev.,* **119,** 1786–1815.

Jones, S. C., and Coauthors, 2003a: The ET of tropical cyclones: Forecast challenges, current understanding, and future directions. *Wea. Forecasting,* **18,** 1052–1092.

——, C. Velden, S. Aberson, J. Abraham, and P. Harr, 2003b: ET, Thorpex, and the North Atlantic TrEC. *Proc. Second Int. Workshop on ET,* Halifax, NS, Canada.

Kalnay, E., and Coauthors, 1996: The NCEP/NCAR 40-Year Reanalysis Project. *Bull. Amer. Meteor. Soc.,* **77,** 437–471.

Kanamitsu, M., 1989: Description of the NMC global data assimilation and forecast system. *Wea. Forecasting,* **4,** 335–342.

Klein, P., P. Harr, and R. L. Elsberry, 2000: ET of western North Pacific tropical cyclones: An overview and conceptual model of the transformation stage. *Wea. Forecasting,* **15,** 373–396.

——, ——, and ——, 2002: Extratropical transition of western North Pacific tropical cyclones: Midlatitude and tropical cyclone contributions to reintensification. *Mon. Wea. Rev.,* **130,** 2240–2259.

Kurihara, Y., R. E. Tuleya, and M. A. Bender, 1998: The GFDL Hurricane Prediction System and Its Performance in the 1995 Hurricane Season. *Mon. Wea. Rev.,* **126,** 1306–1322.

Liu, Q., T. Marchok, H.-L. Pan, M. Bender, and S. Lord, 2000: Improvements in hurricane initialization and forecasting at NCEP with global and regional (GFDL) models. Technical Procedures Bulletin 472 NOAA/NWS, 7 pp. [Available online at http:www.nws.noaa.gov/om/tpb/472.htm, or from NOAA/NWS, 1325 East-West Highway, Silver Spring, MD 20910.]

Ma, S., H. Ritchie, J. Gyakum, J. Abraham, C. Fogarty, and R. McTaggart-Cowan, 2003: A study of the extratropical reintensification of former Hurricane Earl using Canadian Meteorological Centre regional analyses and ensemble forecasts. *Mon. Wea. Rev.,* **131,** 1342–1359.

Maue, R., and R. Hart, 2005: Warm-seclusion extratropical cyclone development: Sensitivity to the nature of the incipient vortex. Preprints, *21st Conf. on Weather Analysis and Forecasting*, Washington, DC, Amer. Meteor. Soc., CD-ROM, P1.16.

McTaggart-Cowan, R., J. R. Gyakum, and M. K. Yau, 2001: Sensitivity testing of ETs using potential vorticity inversions to modify initial conditions: Hurricane Earl case study. *Mon. Wea. Rev.,* **129,** 1617–1636.

——, ——, and ——, 2003: The influence of the downstream state on ET: Hurricane Earl (1998) case study. *Mon. Wea. Rev.,* **131,** 1910–1929.

——, ——, and ——, 2004: The impact of tropical remnants on extratropical cyclogenesis: Case study of Hurricanes Danielle and Earl (1998). *Mon. Wea. Rev.,* **132,** 1933–1951.

Molinari, J., S. Skubis, and D. Vollaro, 1995: External influences on hurricane intensity. Part III: Potential vorticity structure. *J. Atmos. Sci.,* **52,** 3593–3606.

Ritchie, E. A., and R. L. Elsberry, 2001: Simulations of the transformation stage of the extratropical transition of tropical cyclones. *Mon. Wea. Rev.,* **129,** 1462–1480.

——, and ——, 2003: Simulations of the extratropical transition of tropical cyclones: Contributions by midlatitude upper-level trough to reintensification. *Mon. Wea. Rev.,* **131,** 2112–2128.

Sekioka, M., 1957: A hypothesis on complex of tropical and extratropical cyclones for typhoon in the middle latitudes. III. Examples of typhoon not accompanied by extratropical cyclone in the middle latitudes. *J. Meteor. Soc. Japan,* **35,** 170–173.

Shapiro, L. J., and D. Keyser, 1990: Fronts, jet streams, and the tropopause. *Extratropical Cyclones, The Erik Palmen Memorial Volume*, C. W. Newton and E. O. Holopainen, Eds., Amer. Meteor. Soc., 167–191.

Thorncroft, C., and S. C. Jones, 2000: The ET of Hurricanes Felix and Iris in 1995. *Mon. Wea. Rev.,* **128,** 947–972.

Velden, C. S., T. Olander, and S. Wanzong, 1998: The impact of multispectral GOES-8 wind information on Atlantic tropical cyclone track forecasts in 1995. Part I: Dataset methodology, description, and case analysis. *Mon. Wea. Rev.,* **126,** 1202–1218.